Pervaporation Separation of Butanol from Aqueous Solutions Using Polydimethylsiloxane (PDMS) Mixed Matrix Membranes

by

Ali Zamani

uOttawa

Thesis submitted to the Faculty of Graduate and Postdoctoral Studies in partial fulfillment of the requirements for the Master of Applied Science

Department of Chemical and Biological Engineering

Faculty of Engineering

University of Ottawa

Abstract

In this study, pervaporation, a membrane-based process was studied for in-situ separation of butanol. This technique has a great potential due to its high selectivity, low energy requirement and high efficiency. The primary objective was to improve the performance of the Polydimethylsiloxane (PDMS) membrane for the pervaporation separation and the recovery of butanol by adding nanoparticles into its matrix to make mixed matrix membrane (MMM). These nanoparticles included zinc-based Metal Organic Frameworks (MOFs) and zinc oxide. Different particle sizes of zeolitic imidazolate framework (ZIF-8) were synthesized. The separation performance of MMMs incorporating different sizes of ZIF-8 nanoparticles was compared to the performance of mixed matrix membranes incorporating zinc oxide as well as pure PDMS membrane. Different characteristics of ZIF-8 and their impact on the performance of the host membrane were discussed. Result showed that the presence of nanoparticles improves the PDMS membrane performance up to a certain particle loading. Moreover, it was shown that the particle size and interfacial bond between polymer and particles have a major impact on the pervaporation membrane separation process. The best membrane for pervaporation separation of butanol from binary aqueous solutions was obtained for the 8 wt% small-size ZIF-8/PDMS MMM where the total permeation flux and butanol selectivity were increased by 350% and 6%, respectively, compared to neat PDMS membranes.

In addition to the MOFs, nanotubes are considered emerging nanostructured materials for use in membrane separation applications due to their high molecular diffusivity and unique geometry. Recent progress has also been made on the modification of nanotube surface functionality, and the fabrication of nanotube mixed matrix membranes as well as the ability to align them in MMMs. Since numerous types of nanotubes are available and the process of producing well-aligned nanotube MMMs is very challenging, a theoretical model using finite difference method (FD) was used to gain a deeper understanding on the effect of nanotubes on the separation performance of mixed matrix membranes. A series of numerical simulations were performed and the effects of various structural parameters, including the tubular filler volume fraction, orientation, length-to-diameter aspect ratio, and permeability ratio, were assessed. The results showed that the relative permeability is enhanced by vertically-aligned nanotubes and further increased with an increase of the permeability ratio, filler volume fraction and the length-to-diameter aspect ratio.

In addition, comparing the simulation results with existing analytical models for the prediction of the relative permeability acknowledges a need to develop a new correlation that would provide more accurate predictions of the relative permeability of MMMs with embedded nanotube fillers.

Résumé

Dans cette étude, la pervaporation, un procédé membranaire, a été étudiée pour la séparation in situ du butanol. Cette technique présente un grand potentiel en raison de sa bonne sélectivité, de sa faible consommation en énergie et de son rendement élevé. L'objectif principal était d'améliorer les performances des membranes de polydiméthylsiloxane (PDMS) pour la séparation par pervaporation et la récupération de butanol en ajoutant des nanoparticules dans sa matrice pour en faire une membrane à matrice mixte (MMM). Ces nanoparticules possèdent des structures organométalliques à base de zinc et d'oxyde de zinc. Différentes tailles de particules de la structure d'imidazolate zéolitique (ZIF-8) ont été synthétisées. La performance de séparation des MMM incorporant différentes tailles des nanoparticules de ZIF-8 a été comparée aux performances des membranes à matrice mixte incorporant de l'oxyde de zinc ainsi que des membranes de PDMS sans nanoparticules. Les différentes caractéristiques du ZIF-8 et leur impact sur les performances de la membrane hôte ont été discutés. Les résultats ont montré que la présence de nanoparticules améliore les performances de la membrane de PDMS jusqu'à une certaine fraction massique de particules. De plus, il a été démontré que la taille des particules et la qualité de l'interface entre le polymère et les particules ont un impact majeur sur le processus de séparation par membrane de pervaporation. La meilleure membrane pour la séparation par pervaporation du butanol à partir de solutions aqueuses binaires a été obtenue pour les MMM de ZIF-8/PDMS de petite taille avec une teneur de 8% en poids où le flux total de perméation et la sélectivité en butanol ont été augmentés de 350% et 6%, respectivement, par rapport aux membranes PDMS sans nanoparticules.

En plus des MOFs, les nanotubes sont considérés comme des matériaux nanostructurés émergents pouvant être utilisés dans les applications de séparation par membrane en raison de leur grande diffusivité moléculaire et de leur géométrie unique. Des progrès récents ont également été réalisés en ce qui concerne la modification de la fonctionnalité de surface des nanotubes et la fabrication des membranes à matrice mixte incorporant des nanotubes, ainsi que la possibilité de les aligner dans les MMMs. Étant donné que de nombreux types de nanotubes sont disponibles et que la fabrication des MMMs incorporant des nanotubes bien alignés est très difficile, un modèle théorique utilisant la méthode des différences finies (FD) a été utilisé pour comprendre l'effet des nanotubes sur les performances des membranes à matrice mixte. Une série de simulations numériques a été réalisée et les effets de divers paramètres structuraux, notamment la fraction

volumique des nanotubes, l'orientation, le rapport longueur/diamètre et le rapport de perméabilité, ont été évalués. Les résultats ont montré que la perméabilité relative était améliorée par la présence des nanotubes alignés verticalement et augmentait encore plus avec l’augmentation du rapport de perméabilité, la fraction volumique occupée par les nanotubes et le rapport hauteur/diamètre. En outre, la comparaison des résultats de la simulation avec les modèles analytiques existants pour la prédiction de la perméabilité relative reconnaît le besoin de développer de nouvelles corrélations fournissant des prédictions plus précises de la perméabilité relative des MMMs incorporant des nanotubes.

Statement of Contributions

Chapter 2, entitled “Separation of n-Butanol from Aqueous Solutions via Pervaporation Using PDMS/ZIF-8 Mixed Matrix Membranes of Different Particle Sizes”, was thoroughly suggested by me. I proposed the use of metal-organic frameworks and performed all experiments and analysis. I wrote the first draft of the paper and made numerous revisions based on the comments from Dr. Jules Thibault and Dr. Handan Tezel.

Chapter3, entitled “Modeling the molecular permeation through mixed matrix membranes incorporating tubular fillers” was proposed by me. The idea of using the OpenFOAM in conjunction with the finite difference method was suggested by me. The finite difference method was initially coded by Dr. Jules Thibault in the FORTRAN, then further developed by me. I performed numerous simulations and wrote the first draft of the paper. The draft was revised by me with constructive comments from Dr. Jules Thibault and Dr. Handan Tezel.

Acknowledgments

First and foremost, I would like to thank my supervisors Dr. Jules Thibault and Dr. Handan Tezel for their patient guidance, encouragement and advice they have provided throughout my time as their student. It would absolutely not be possible to complete this thesis without their continuous support, insights and help.

I would like to extend my sincerest thanks and appreciation to my family especially my wife, for their supports, encouragement and patience during my pursuit of the M.A.Sc program in chemical engineering.

I would like to acknowledge Natural Science and Engineering Research Council (NSERC) of Canada for providing the financial support for this work.

Table of Contents

List of Figures

List of Tables

Chapter 1:

Introduction and structure of the thesis

1.1 Introduction

Biofuels have been considered as a renewable and environment-friendly energy source that can partially replace the conventional petroleum-based energy [1]. In particular, biobutanol has gained increasing attention as one of the most valuable biofuels due to its high energy density, relatively low volatility, ease of transport and ability to form high-level blends with petroleum [2]. Biobutanol is typically produced via acetone-butanol-ethanol (ABE) fermentation using renewable feedstocks. However, this fermentation process mainly requires high cost starch-based materials and produces a very low butanol concentration due to its high toxicity to the cells [3]. Numerous separation techniques were proposed for their integration with the fermentation process for the in-situ removal of butanol from the fermentation broth to overcome the inhibition effect and to prolong the continuous fermentation, thus leading a more cost-effective biobutanol production [4].

Among the existing in-situ separation technologies, pervaporation (PV), a membrane-based process, was suggested as a promising method for butanol separation owing to its advantages in energy-efficiency and less harmful effects on microorganisms [5]. In membrane pervaporation, a liquid mixture is in contact with a dense membrane on the feed side and some species are allowed to permeate to the other side of the membrane where they are removed as vapour. The permeate side of the membrane is held under vacuum or a sweep gas to maintain a very low pressure in order to create a concentration gradient across the membrane [3].

One of the key drivers of the pervaporation process is developing highly permeable, selective and stable membranes. Various membranes have been studied for recovering butanol from aqueous solution, including polydimethylsiloxane (PDMS) [6], poly(ether block amide) (PEBA) [7], poly[1-(trimethylsilyl)-1-propyne] (PTMSP) [7] and liquid membranes [8]. Among them, PDMS membranes are the most commonly used owing to their good hydrophobicity, processibility and stability. However, these types of membranes are suffering from the trade-off between permeability and selectivity. Mixed matrix membranes (MMMs), comprising a filler phase embedded into a polymer matrix, have emerged in an attempt to partly overcome some of the

limitations of conventional polymer and inorganic membranes. MMMs are made by embedding a proper organic or inorganic filler in the polymer matrix, and potentially combining the advantages of the higher selectivity of the filler particles and the ease of processing of polymers [3,6].

While there are numerous types of fillers and polymers available, a rational choice of both phases toward the preparation of MMMs is necessary. The main objectives of this study were to improve the performance of the PDMS membrane for the pervaporation separation and the recovery of butanol from aqueous solution as well as identifying the main features of a beneficial filler. These objectives were undertaken with two distinct but related studies. The first part was experimental, in which zeolitic imidazolate framework (ZIF-8) was embedded in PDMS matrix to evaluate the MMM's butanol separation performance. ZIF-8 was chosen in this study due to its unique synthetizing method that gives the advantage of controlling the particle sizes. Also, ZIF-8 high stability in water and alcohols, in contrast to the most MOFs, makes it very suitable in this application [9].

In addition to the MOFs, nanotubes are other nanomaterials that are advantageous for their use in membrane separation applications due to their high molecular diffusivity and unique geometry [10]. Recent progress has also been made on the fabrication of mixed matrix membrane embedding nanotubes as well as the ability to align them in MMMs [11]. Since numerous types of nanotubes are available and the process of producing well-aligned nanotubes within MMMs is very challenging and reliant to its inherent properties, a theoretical model using a finite difference method (FD) was used in the second part of this study to investigate their effects on the performance of mixed matrix membranes. A series of numerical simulations were performed and the effects of various structural parameters, including the tubular filler volume fraction, orientation, aspect ratio, and permeability ratio, were assessed.

1.2 Research objectives

The main objectives of this project are:

1. To improve the performance of PDMS membranes for the pervaporation separation of butanol from binary aqueous solutions by developing an efficient membrane to achieve a high selectivity as well as a high butanol permeation flux.

2. To investigate the effect of the filler properties such as: shape, size and its concentration in mixed matrix membrane on the pervaporation separation of butanol in terms of butanol permeation flux and selectivity.
3. To investigate the potential use of aligned-nanotube fillers in mixed matrix membranes by developing a mathematical model to gain a deeper understanding of the effects of structural parameters, including the orientation, aspect ratio, and permeability ratio.

1.3 Thesis structure

The main body of this thesis is comprised of four chapters: introduction, butanol pervaporation separation from binary aqueous solutions, modeling the pervaporation process where MMMs are used, and the conclusions and recommendations.

Chapter 1 presents some background information on the research considered in this thesis as well as the objectives and the structure of the thesis. **Chapter 2** presents a study on the effect of the particle size and shape, as well as loading content of the ZIF-8 nanoparticles on the performance of the PDMS membrane for pervaporation separation of the butanol from binary aqueous solutions. **Chapter 3** presents the results of a numerical study to predict the mass transport of the components through a mixed matrix membrane incorporating tubular filler with different orientation and assess the membrane performance as a function of numerous factors. **Chapter 4** provides some overall conclusions of the research undertaken in this thesis as well as some recommendations for future work.

1.4 References

[1] J.Y. Lee, S.O. Hwang, H.J. Kim, D.Y. Hong, J.S. Lee, J.H. Lee, Hydrosilylation-based UV-curable polydimethylsiloxane pervaporation membranes for n-butanol recovery, Sep. Purif. Technol. 209 (2019) 383–391. doi:10.1016/j.seppur.2018.07.045.

[2] P.P. Peralta-Yahya, J.D. Keasling, Advanced biofuel production in microbes, Biotechnol. J. 5 (2010) 147–162. doi:10.1002/biot.200900220.

[3] H. Azimi, A. Ebneyamini, F.H. Tezel, J. Thibault, Separation of organic compounds from ABE model solutions via pervaporation using activated carbon/PDMS mixed matrix membranes, Membranes (Basel). 8 (2018) 1–15. doi:10.3390/membranes8030040.

[4] Y. Pan, Y. Hang, X. Zhao, G. Liu, W. Jin, Optimizing separation performance and interfacial adhesion of PDMS/PVDF composite membranes for butanol recovery from aqueous solution, J. Memb. Sci. 579 (2019) 210–218. doi:10.1016/j.memsci.2019.03.008.

[5] H. Zhu, G. Liu, J. Yuan, T. Chen, F. Xin, M. Jiang, Y. Fan, W. Jin, In-situ recovery of bio-butanol from glycerol fermentation using PDMS/ceramic composite membrane, Sep. Purif. Technol. 229 (2019) 115811. doi:10.1016/j.seppur.2019.115811.

[6] H. Azimi, F.H. Tezel, J. Thibault, Effect of embedded activated carbon nanoparticles on the performance of polydimethylsiloxane (PDMS) membrane for pervaporation separation of butanol, J. Chem. Technol. Biotechnol. 92 (2017) 2901–2911. doi:10.1002/jctb.5306.

[7] Y. Li, J. Shen, K. Guan, G. Liu, H. Zhou, W. Jin, PEBA/ceramic hollow fiber composite membrane for high-efficiency recovery of bio-butanol via pervaporation, J. Memb. Sci. 510 (2016) 338–347. doi:10.1016/j.memsci.2016.03.013.

[8] H.R. Cascon, S.K. Choudhari, 1-Butanol pervaporation performance and intrinsic stability of phosphonium and ammonium ionic liquid-based supported liquid membranes, J. Memb. Sci. 429 (2013) 214–224. doi:10.1016/j.memsci.2012.11.028.

[9] H. Zhang, D. Liu, Y. Yao, B. Zhang, Y.S. Lin, Stability of ZIF-8 membranes and crystalline powders in water at room temperature, J. Memb. Sci. 485 (2015) 103–111. doi:10.1016/j.memsci.2015.03.023.

[10] T. P. Wang, D.Y. Kang, Predictions of effective diffusivity of mixed matrix membranes with tubular fillers, J. Memb. Sci. 485 (2015) 123–131. doi:10.1016/j.memsci.2015.03.028.

[11] D. Yang, C. Cheng, M. Bao, L. Chen, Y. Bao, C. Xue, The pervaporative membrane with vertically aligned carbon nanotube nanochannel for enhancing butanol recovery, J. Memb. Sci. 577 (2019) 51–59. doi:10.1016/j.memsci.2019.01.032.

Chapter 2:

Separation of n-Butanol from Aqueous Solutions via Pervaporation Using PDMS/ZIF-8 Mixed Matrix Membranes of Different Particle Sizes

Ali Zamani, Jules Thibault, F. Handan Tezel

Department of Chemical and Biological Engineering

University of Ottawa, Ottawa, Ontario, Canada K1N 6N5

Abstract

The separation of biofuels using mixed matrix membranes (MMMs) has attracted significant research interest in the field of renewable energy. In this study, the pervaporation separation of butanol from aqueous solutions was studied using a series of MMMs including zeolitic imidazolate frameworks (ZIF-8)-polydimethylsiloxane (PDMS) and zinc oxide-PDMS mixed matrix membranes. Although several studies have reported that mixed matrix membranes incorporating ZIF-8 nanoparticles showed improved pervaporation performances attributed to its intrinsic micro porosity and high specific surface area, an in-depth study on the role of ZIF-8 nanoparticle size in MMMs has not yet been reported. In this study, different average sizes of ZIF-8 nanoparticles (30, 65, and 80 nm) were synthesized and the effects of particle size and particle loading content on the performance of butanol separation using MMMs were investigated. Furthermore, zinc oxide nanoparticles, as non-porous fillers with the same metal core as ZIF-8 but with a very different geometric shape, were used to illustrate the importance of the particle geometry on the membrane performance. Results showed that small-sized ZIF-8 nanoparticles have better permeability and selectivity than medium and large-size ZIF-8 MMMs. While the permeation flux increased continuously, with an increase in the loading of nanoparticles, the selectivity reached a maximum for MMM with 8 wt % smaller-size ZIF-8 nanoparticle loading. The flux and butanol selectivity increased by 350% and 6%, respectively, in comparison to those of neat PDMS membranes prepared in this study.

2.1 Introduction

Global energy demands are primarily met through non-renewable sources such as oil, coal, and natural gas. However, the scarcity and rising prices of fossil fuels, coupled with the environmental problems facing society, stimulate the vigorous search towards biofuels as viable alternatives to petroleum and other non-renewable fuel products. Biofuels have numerous advantages that can accelerate their adoption worldwide. They open the door of opportunity for renewable transportation fuels, reduce GHG emissions and broaden the global market for agricultural products [1]. Production of biofuels could also improve the economic status of local workers by providing employment opportunities. Of all liquid biofuel alternatives, biobutanol recently received increased attention as a plausible green fuel for the partial replacement of petroleum-based fuels as it possesses fuel properties that are closed to those of gasoline [2]. Biobutanol has desirable fuel characteristics such as low water solubility and vapour pressure, high energy density and cetane number. It can directly be used in existing car engines without any modifications. It has a high miscibility favouring its efficient blending with other fuels. As a result, biobutanol is well-suited for automotive fuel applications [3].

In 1912, Chaim Weizmann discovered a microorganism called *Clostridium acetobutylicum*, which was able to ferment starch to acetone, butanol, and ethanol [4]. The *Clostridium* bacteria is a strict anaerobe and spore-forming microbe, and has been used since to produce various bio-solvents by anaerobic fermentation of numerous monosaccharides and hydrolysate of oligosaccharides [5]. This process, which is called ABE fermentation, can produce acetone, butanol, and ethanol in a typical ratio of 6:3:1, respectively. In this fermentation, 9-12 $g.L^{-1}$ butanol is typically produced while 40–60 $g.L^{-1}$ glucose is consumed under batch conditions [5,6]. Various cellulosic feedstocks are currently being used for biobutanol production such as wheat and barley straw, corn stover, cassava bagasse, switchgrass, and miscanthus in addition to expensive edible feedstocks like glucose and corn starch [6]. Even though improvements have been achieved for this process, currently the ABE fermentation process cannot compete on a commercial scale with petroleum-based butanol produced by hydrolysis of haloalkanes or hydration of alkenes [7]. There are significant challenges to produce this alcohol as an economically viable biofuel. The most important challenge is the inhibition effect on the microorganism by the solvent product at concentrations in the vicinity of 1 wt% [8]. Because of the low butanol concentration caused by

butanol toxicity, the economics of the process are greatly hampered when energy-intensive separation methods such as distillation are used for separating butanol from its dilute aqueous solution [9].

To address the low concentration butanol challenge, it has been recommended to resort to in-situ separation techniques to partially remove solvent products, especially butanol as the most toxic product, during the fermentation process. This in-situ removal allows to obtain higher overall solvent concentrations and increases productivity. Technologies such as gas stripping, liquid-liquid extraction, vacuum stripping, membrane distillation and adsorption can be used in butanol in-situ separation. Another interesting technique to separate butanol from dilute aqueous mixtures is via membrane pervaporation (PV). In membrane pervaporation, a liquid mixture is in contact with a dense membrane on the feed side and some species are allowed to permeate to the other side of the membrane where they are removed as vapour. The permeate side of the membrane is held under vacuum or a sweep gas is used to maintain a very low pressure in order to create a concentration gradient across the membrane [10]. Polymeric membranes have been the most frequently used pervaporation membranes due to their low cost, ease of manufacture and their ability to scale-up.

Polydimethylsiloxane (PDMS) is recognized as a benchmark for alcohol selective membrane material, it is the most commonly used hydrophobic membrane material in PV process due to its significant advantages of good film-forming ability, high permeability to small molecules and chemical stability. Unfortunately, the performance of polymeric membranes such as PDMS is limited by the well-known trade-off effect between permeability and selectivity, where an increase in the former results in decreasing the latter, and vice versa [11]. In recent years, research has focused on fabricating mixed matrix membranes (MMMs) to reduce this trade-off effect. Mixed matrix membranes are manufactured by incorporating various porous or nonporous fillers into the polymer matrix to manipulate the synergistic effect between the polymer and filler phases [12]. A wide range of porous fillers, including zeolites [13], metal-organic frameworks (MOFs) [14], activated carbons (ACs) [15], and carbon nanotubes (CNTs) [16] have been used in mixed matrix membranes. The permeation mechanism prevailing in mixed matrix membranes is not yet completely known. It is hypothesized that some porous fillers offer a lower resistance for some diffusing species and may provide molecular sieving depending on their pore sizes. ZIF-8 is one

of the most widely investigated Zeolitic Imidazolate Frameworks (ZIFs) among metal-organic frameworks family and has extraordinary advantages in alcohol separation. ZIF-8 possesses a sodalite (SOD) zeolite-type structure with a small pore aperture of a nominal diameter of ~3.4 Å and an effective aperture size in the range of 4.0–4.2 Å due to its flexible framework [17]. ZIF-8 could form preferential butanol channels contributed by a sub-nanometer scale hydrophobic interconnected structure that is favourable for fast butanol transport. Furthermore, ZIF-8 has additional advantages, namely its low cost, raw materials availability, simple preparation method, and tunable size and morphology [18]. Moreover, ZIF-8 shows high water stability, which is vital for water-related applications [19]. It is known that the separation performances of ZIF-8/PDMS mixed matrix membranes highly depend on the intrinsic properties of the ZIF-8 and the PDMS, the interaction between the two and the percentage of ZIF-8 loading in the mixed matrix membrane [20]. However, the possible effect of the ZIF-8 particle size on the permeation characteristics of the ZIF-8 filled polymeric membranes has not yet been investigated. In this study, different loadings of ZIF-8/PDMS were prepared to seek optimum performance for the separation of biobutanol using mixed matrix membranes. In addition, different particle sizes of ZIF-8 were synthesized and incorporated into the matrix of the PDMS membranes to study the effects of the particle size on the performance of PDMS MMMs for the separation of butanol from aqueous binary solutions.

2.2 Materials and Methods

2.2.1 Materials

Polydimethylsiloxane (PDMS) and cross-linking agent kit (RTV615 001 KIT) were obtained from Momentive Co. (Hebron, Ohio, USA). Polyacrylonitrile (PAN) membranes, used as a support for PDMS in this study, were purchased from Synder Filtration (Vacaville, California, USA) with 30 000 Da molecular weight cut-off and a thickness of 0.15 mm (Polyester + PAN). Zinc Nitrate Hexahydrate ($Zn(NO_3)_2 \cdot 6H_2O$), 2- Methylimidazole (Hmim, 99%) and Sodium Hydroxide (NaOH) were purchased from Sigma Aldrich (Ottawa, Ontario, Canada). Methanol (99.9% purity), Butanol (99% purity) and Tetrahydrofuran (THF) were obtained from Fisher Scientific Inc. (Ottawa, Ontario, Canada). All reagents were used as received without further purification and deionized distilled water was used to prepare all aqueous solutions.

2.2.2 Nanoparticles synthesis

2.2.2.1 ZIF-8 nanoparticles

ZIF-8 was synthesized based on a similar synthesis protocol described by Demir et al. [21], using Zinc Nitrate Hexahydrate ($Zn(NO_3)_2.6H_2O$), 2-Methyl Imidazole (Hmim), and methanol. In this method, Zinc Nitrate Hexahydrate and Hmim were dissolved in separate beakers containing half of the total amount of methanol by stirring at room temperature for 15 min at 300 rpm. These two beakers were then combined into one, to initiate the synthesis of the MOF particles. ZIF-8 synthesis was immediately started by mixing both reactants together and continued for one hour at 300 rpm at room temperature to form a milky white solution. The particles were then separated from the synthesis solution by centrifugation at 6000 rpm for 5 min. The resulting supernatant liquid, referred to as the mother liquor, was put aside and recycled to produce more ZIF-8 particles with the addition of sodium hydroxide. The separated particles were then washed with deionized distilled water and re-separated by centrifugation at 6000 rpm for 20 min. The washing-centrifugation process was performed three times. The particles were then placed in an oven, and dried at 80°C for 12 h. Low temperature calcination, which is sometimes referred to as annealing, was then conducted by placing the particles in a preheated oven at 180°C for 12 h with no additional time for heating and cooling. For the ZIF-8 particles fabricated in this study, ZIF-8-1 particles were fabricated using the above procedure. ZIF-8-2 particles were fabricated using the mother liquor from the fabrication of particles ZIF-8-1 in combination with additional solid NaOH as the synthesis solution. Furthermore, ZIF-8-3 particles were fabricated using the mother liquor from the fabrication of particles ZIF-8-2 with added Zinc Nitrate Hexahydrate as the synthesis solution. The synthesis solutions for ZIF-8-2 and ZIF-8-3 particles were then aged at room temperature by stirring the solution for one hour at 300 rpm. The particles were then separated, washed, dried, and calcined the same way as for ZIF-8-1 particles in this study.

2.2.2.2 Zinc Oxide (ZnO) particles

ZnO particles were prepared using the method outlined previously by Wu et al. [22] with some modifications. In this method, the alkali solution of zinc was prepared by dissolving 2.5 g of Zinc Nitrate Hexahydrate and 3.5 g NaOH in two separate 80 mL deionized water at room temperature. Then, the NaOH solution was heated to 30°C and the Zinc Nitrate solution was added dropwise under constant stirring. After stirring for 2 h at 300 rpm and 30°C, the white precipitate that settled

at the bottom of the beaker was collected by centrifugation at 6000 rpm for 5 min. The ZnO particles were then washed with methanol and re-separated by centrifugation two more times before being dried at 80°C for 12 h.

2.2.3 Fabrication of MMMs

2.2.3.1 Neat membrane

Neat PDMS membranes were prepared using the method outlined by Azimi et al. [10]. PAN membranes, which are known to have high porosity, were used as backing material to deposit a thin PDMS layer. The PAN membrane was taped on a glass plate after being thoroughly rinsed with water. The PDMS solution for the active layer was prepared by mixing 5 g of the base PDMS solution from the silicone kit in 20 g of THF. The solution was mixed using a stirrer (RZR 2102, Heidolph Electronic, Wood Dale, Illinois, USA) for 30 min and then 0.5 g of the crosslinking agent was added to this mixture and stirred for an additional 45 min. The PDMS solution was then sprayed onto the PAN membrane using an air pen brush (Paasche VL-SET Double Action Siphon Feed Airbrush, Kenosha, Wisconsin, USA) in two successive layers. The main solution was first sprayed as uniformly as possible in one direction onto the PAN support and, following a 10 min period under vacuum condition, the membrane was turned 90° and a second layer was sprayed akin to the first layer. The glass plate with the membrane was then placed in a vacuum oven. The vacuum oven was maintained at an absolute pressure of 0.2 bar for 30 min at room temperature, and then the oven was heated up to 90°C for 3 h including the pre-heating period while maintaining the same vacuum pressure. Following this curing procedure, the membrane was taken out of the oven and cooled to room temperature.

2.2.3.2 ZIF-8 and ZnO nanoparticles filled PDMS mixed matrix membranes

To fabricate the mixed matrix membranes, a procedure similar to the one mentioned in Section 2.2.3.1 for the neat PDMS membrane was followed. However, certain weight percent of ZIF-8 nanoparticles were added to the main solution for the preparation of the membrane. The nanoparticle percentages were evaluated using Equation (2.1).

$$\text{ZIF} - 8\ (\text{wt}\%) = \frac{W_{ZIF-8}}{W_{ZIF-8} + W_{PDMS}} \times 100 \qquad (2.1)$$

where $W_{ZIF\text{-}8}$ and W_{PDMS} are the weights of the nanoparticle and the base PDMS from the silicon kit in the membrane casting solution.

The nanoparticles were first thoroughly mixed within 20 g of THF using a sonicator (QSONICA, Part No.Q700, Newtown, Connecticut, USA) at 0°C temperature for 1 h. Then, 5 g of PDMS was added to the mixture and mixed for 30 min at room temperature. Next, 0.5 g of the crosslinking agent was added and stirred for 45 min at room temperature. The same procedure described in Section 2.2.3.1 was then used to apply the two successive layers of the ZIF-8/PDMS solution, including the subsequent curing of the membrane. Noteworthy, the spray nozzle was large enough to spray the solution without any clogging and to ensure that the ZIF-8/PDMS solutions were sprayed uniformly. The same procedure was used to fabricate ZIF-8/PDMS and ZnO/PDMS membranes with different particle sizes.

2.2.4 Characterization of nanoparticles and membranes

Images of the membranes were taken using a scanning electron microscope (SEM, JSM-7500F, Peabody, Massachusetts, USA). Each sample was freeze-fractured after immersion in liquid nitrogen and was then taped on a support using a carbon tape to fix the sample. The sample was gold sputtered before SEM observations were made. Powder X-ray diffraction (XRD) patterns of ZIF-8 particles were acquired using a Max Rigaku X-ray diffractometer with a copper anode and a graphite monochromator to select Cu-Kα radiation (λ=1.540 Å), taking data from $2\theta = 0°$ to 80° at a scan rate of 1°/s. Transmission electron microscopy (TEM) was performed on a FEI Tecnai G2 Spirit Twin and operated at 120 kV. The samples were dispersed in THF and loaded on a 50 nm 300-mesh carbon-coated copper grids.

A digital micrometer caliper (0-1", Mitutoyo, Aurora, Illinois, USA) was used to measure the membrane thickness. Measurements were made at five different spots and the average was reported. The hydrophobicity/organophilicity of the membrane surface was characterized by the static and dynamic contact angle measurements. The static contact angle (SCA) was measured using the video optima surface analysis system (Optima AST Product Inc., Billerica, Massachusetts, USA) by placing 3 μL droplet of the solution on the membrane surface.

The machine is able to capture static and dynamic pictures of the droplet and calculates the surface contact angle by determining the tangent lines. For each membrane, the static contact angle was measured at five different locations and the values were averaged. The static contact angle was measured for pure water and for a 5 $g.L^{-1}$ butanol aqueous solution. The dynamic contact angle of pure butanol was measured by recording 10 frames for 1 min considering the rapid change of butanol droplet contact angle at the surface due to butanol evaporation and impregnation.

2.2.5 PV experiments

Permeation experiments were carried out using the pervaporation experimental setup presented in Figure 2.1 [15]. The setup consists of three membrane modules placed in series where the retentate from each membrane was directed to the next one. The three-module membrane system was placed in a temperature-controlled oven accompanied by a long stainless-steel coil to ensure the feed stream reaches the desired temperature prior to entering the first membrane module. Furthermore, a thermocouple was used to measure the feed temperature halfway between the coil and first membrane to confirm that the temperature reached its desired value. The vapour phase streams exiting the permeate side of each membrane modules were collected in individual cold traps. Cold traps were immersed into liquid nitrogen Dewar accompanied by an automatic time-fill controller to maintain a pre-set liquid nitrogen level (Gordinier Electronics Inc, model 359 liquid time fill, Roseville, Michigan, USA). The permeate side of the three membrane modules and the three cold traps were maintained at very low pressure (1 Torr) using a vacuum pump (Scroll Pump, 78603-11, Cole-Parmer, Montreal, Quebec, Canada). A digital pressure gauge was used after the cold traps to monitor the vacuum pressure. At the end of each experiment, the permeation rate was determined gravimetrically by weighing the permeate sample collected over a given period of time. Both the feed and permeate compositions were analyzed by a liquid density meter (DMA 4500 M, Anton Paar, Saint-Laurent, Quebec, Canada). In some cases, the content of butanol in the permeate exceeded its solubility limit at room temperature, and the permeate sample formed two phases. Under these circumstances, the permeate sample was diluted with deionized water when determining the overall permeate composition. Initially, the butanol concentration in the feed was fixed at 5 $g.L^{-1}$, and during a pervaporation run, the quantity of permeate removed by the membrane was kept below 1% of the initial feed load to maintain an essentially constant feed composition. Since the reference feed temperature of ABE fermentation broth is usually between

37-40°C, the feed temperature was considered constant at 39°C. All the experimental data reported were obtained at steady-state pervaporation.

The permeation flux, selectivity and permeability were used to characterize the membrane performance. The flux (J) is the permeate flow rate per unit membrane surface area, which is normally determined for each species from the total permeation flux and permeate mass fraction of each component. The membrane selectivity can be characterized by the separation factor, which is a metric that assesses the separation ability of the membrane considering two substances to be separated. The permeability allows the comparison of the membrane's performance with different properties.

These performance parameters for individual species *i* are defined in Equations (2.2)-(2.4).

$$J_i = {m_i}/{A.t} \tag{2.2}$$

$$\alpha_i = \frac{{y_i}/{1 - y_i}}{{x_i}/{1 - x_i}} \tag{2.3}$$

$$P_i = \frac{J_i.\sigma}{C_{i-feed} - C_{i-permeate}} \tag{2.4}$$

where m_i is the mass of component *i* in the permeate stream (g), *A* is the effective surface area of the membrane (m^2), *t* is the time of permeation (h), y_i and x_i are the mass fraction of component *i* in the permeate and feed streams, respectively. P_i is the permeability and σ is the effective thickness of the membrane. C_{i-feed} and $C_{i-permeate}$ are the concentrations of component *i* in the feed and permeate side, respectively ($g.L^{-1}$). By assuming high vacuum on permeate side, it can be assumed that $C_{i-permeate}$ is equal to zero.

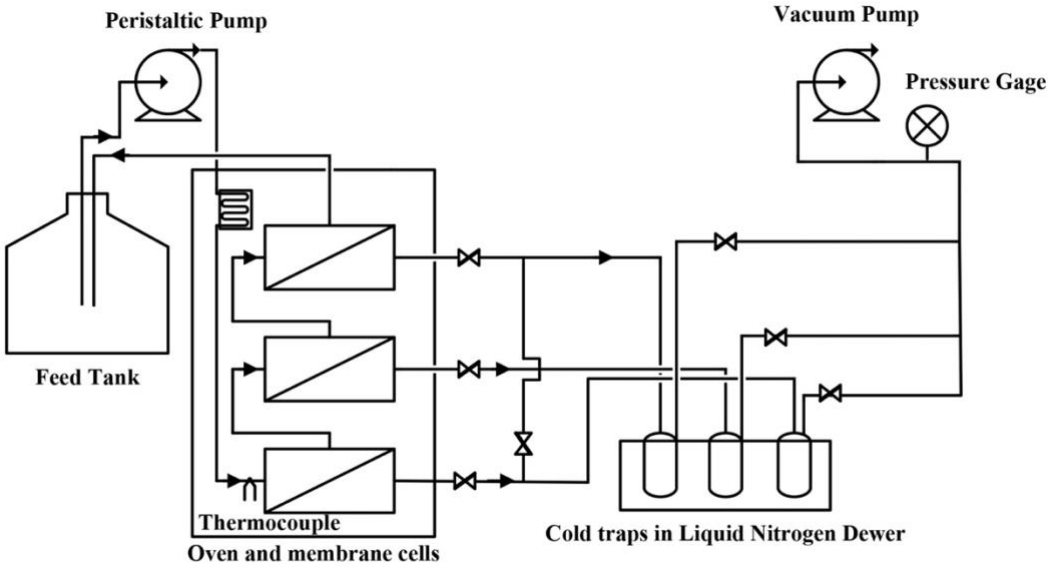

Figure 2.1. Schematic diagram of the pervaporation experimental setup [15].

2.3 Results and discussion

2.3.1 Characterization of ZIF-8 and ZnO nanoparticles

ZnO and three different sizes of ZIF-8 (i.e. ZIF-8-1, ZIF-8-2, ZIF-8-3) were synthesized and characterized before using them as fillers in PDMS-based MMMs. Representative TEM images of the different samples are presented in Figure 2.2, where the different particle sizes and morphologies are compared. While the smallest ZIF-8 particles (ZIF-8-3) are almost spherical, the largest particles (ZIF-8-1) have well defined edges with the typical rhombic dodecahedron shape of ZIF-8 that has been suggested by Demir et al. [21]. In addition, the rod-like shape of ZnO is consistent with the geometry that was reported in literature [22]. A statistical size evaluation using more than 100 nanoparticles of ZIF-8 indicates that the average size of ZIF-8-1, ZIF-8-2 and ZIF-8-3 nanoparticles were approximately 80±20, 65±8 and 30±15 nm, respectively, as listed in Table 2.1. The relatively small particle sizes of all three ZIF-8 is considered as an advantage for the successful fabrication of defect-free mixed matrix membranes. The XRD patterns of ZIF-8-1, ZIF-8-2 and ZIF-8-3 MOFs with sizes between 30 and 80 nm are represented in Figure 2.3. All samples indicate a pattern with identical shape and peaks at the same positions, acknowledging

that they constitute the same kind of MOF. Moreover, the height and width of the different peaks is equivalent for all samples, disregarding their size, which also indicates high crystallinity. Furthermore, the XRD pattern for ZnO is provided in Figure 2.4 to ensure the identical crystallinity with the standard.

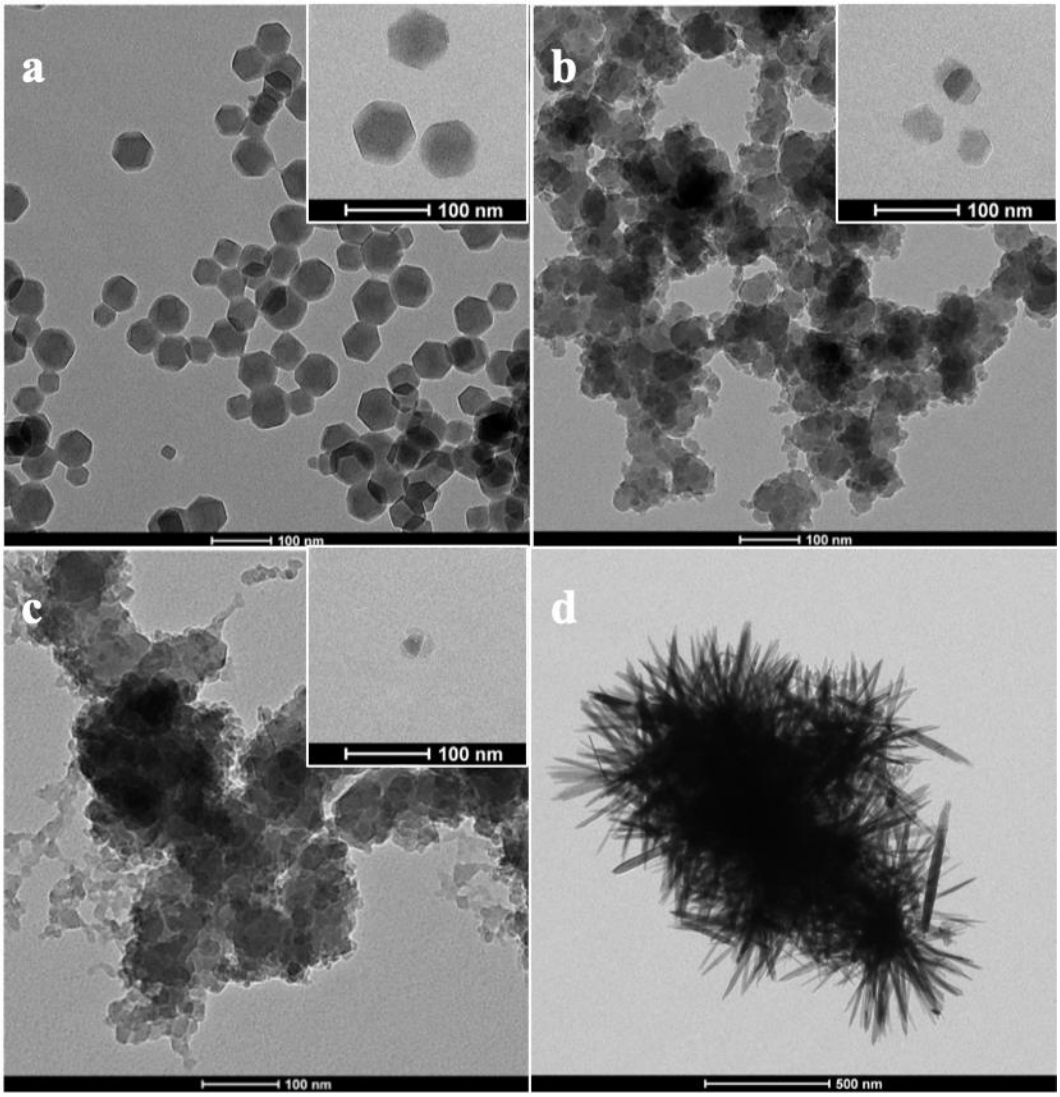

Figure 2.2. TEM images for: **(a)** ZIF-8-1 nanoparticles, **(b)** ZIF-8-2 nanoparticles, **(c)** ZIF-8-3 nanoparticles and **(d)** ZnO particles.

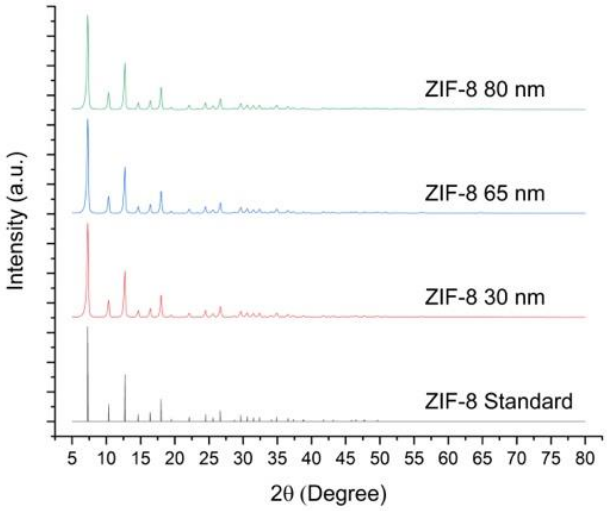

Figure 2.3. XRD patterns of ZIF-8, which were synthesized in different particle sizes. The ZIF-8 standard data represent the simulation pattern obtained from Cambridge Crystallographic Data Center.

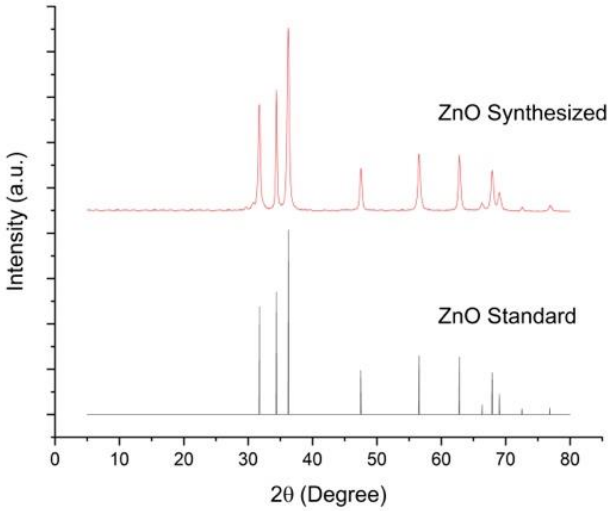

Figure 2.4. XRD patterns of synthesized ZnO particles. The ZnO standard data represent the simulation pattern obtained from Cambridge Crystallographic Data Center.

Table 2.1. Different particle sizes of ZIF-8 and ZnO synthesized in this study.

Particle name	Particle size (nm)
ZIF-8-1	80±20
ZIF-8-2	65±08
ZIF-8-3	30±15
ZnO	500±100

2.3.2 Morphology of ZIF-8/PDMS MMMs

SEM was used to visualize the surface and cross-sectional structure of the membranes prepared. As shown in Figure 2.5, the pure PDMS and 8 wt% ZIF-8-1/PDMS membranes have smooth surfaces compared to 8% ZnO/PDMS membranes. ZIF-8/PDMS smoothness confirms a homogeneous and defect-free MMM surface as well as good interface compatibility between ZIF-8 and hydrophobic PDMS phase. On the other hand, the complex rod-like shape of ZnO may contribute to the rough surface of ZnO/PDMS membranes, which led to a larger surface area. The SEM surface image analysis was also done for all the other MMMs including different ZIF-8 particle sizes and since their surface images were similar and as smooth as pure PDMS, those SEM surface pictures are not included. Figure 2.6(a) presents the SEM image of the cross-section of the pure PDMS membrane, which consists of three layers: 1. Dense PDMS layer at the top corresponding to the effective or active layer, 2. PAN porous support layer and 3. Polyester layer. The last two layers are identical for all MMMs manufactured in this study and referred to as the PAN support. Figure 2.6(b) shows that a certain level of agglomeration prevails on the cross-sectional area of the ZIF-8-1/PDMS MMM, which may be attributed to the bigger particle sizes and non-uniform distribution of ZIF-8. In comparison, fewer particle agglomerations were observed in cross-sectional pictures of ZIF-8-2, ZIF-8-3, and ZnO/PDMS MMMs. In general, a good compatibility between ZIF-8 particles and PDMS polymer chains as well as a homogeneous distribution of smaller particle sizes in PDMS layer were obtained. However, as previously showed in Figure 2.2(d), the complex geometry of ZnO, especially when agglomeration occurs, makes it difficult for the viscous PDMS solution to penetrate and cover the surface area of all the nanoparticles. This poor PDMS solution penetration leads to a higher permeability but at the expense of lower selectivity as a result of these voids and defects.

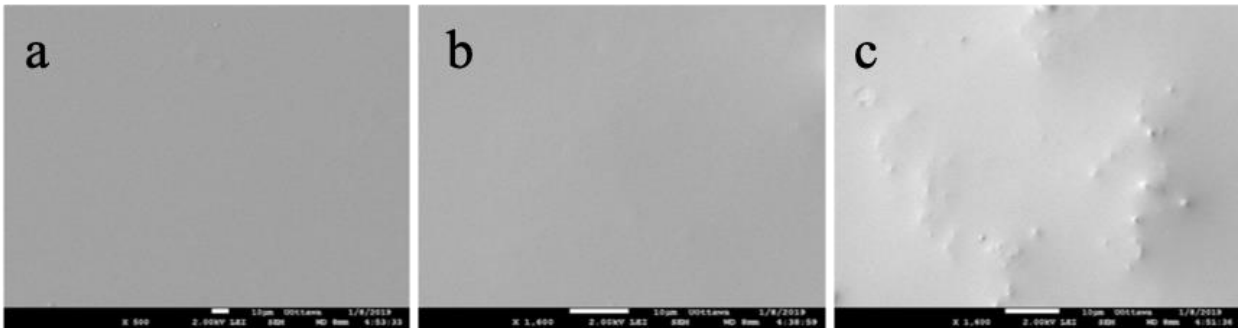

Figure 2.5. SEM images of the surface of the membrane: **(a)** Neat PDMS, **(b)** 8 wt% ZIF-8-1/PDMS and **(c)** 8 wt% ZnO/PDMS.

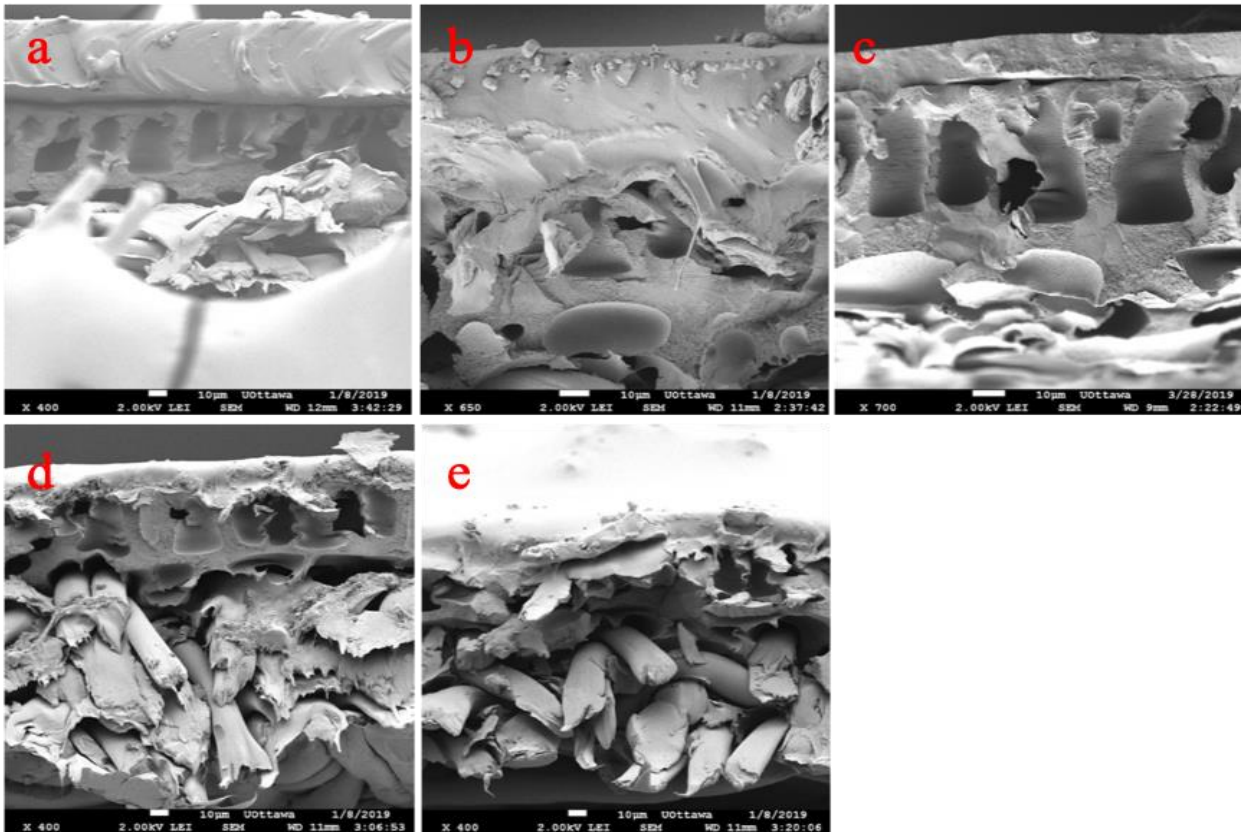

Figure 2.6. SEM cross-section images of **(a)** neat PDMS, **(b)** 8 wt% ZIF-8-1/PDMS, **(c)** 8 wt% ZIF-8-2/PDMS, **(d)** 8 wt% ZIF-8-3/PDMS and **(e)** ZnO/PDMS.

2.3.3 Surface hydrophobicity

The static contact angle measurements were performed to investigate the hydrophobic and organophilic properties of the membranes prepared. Figure 2.7 presents the static contact angles for pure water and 0.5 wt% butanol aqueous solution for the neat PDMS membrane, ZIF-8/PDMS MMMs and ZnO/PDMS MMMs with different particle loadings and particle sizes. The pure PDMS membrane had a static water contact angle of 128° that shows its favourable intrinsic hydrophobicity. There were no significant differences in the water contact angle between different particle sizes of ZIF-8/PDMS MMMs, with slightly lower values than those for the neat PDMS membranes. The water contact angle continued to decrease with increasing ZIF-8 loading, indicating the diminished hydrophobicity of the PDMS membrane after incorporating ZIF-8 particles. In the case of ZnO/PDMS membranes, the agglomeration of small-scale nanorods caused by particles' geometry can affect the surface properties and eventually decrease the water contact angle. Furthermore, the dynamic contact angle was used to measure the butanol contact angle for different particle sizes for 1 min. As Figure 2.8 denotes, neat PDMS membranes exhibited the lowest dynamic contact angle as expected, and ZIF-8-3/PDMS showed better organophilic behaviour than bigger particle sizes of ZIF-8 indicating a better affinity towards butanol.

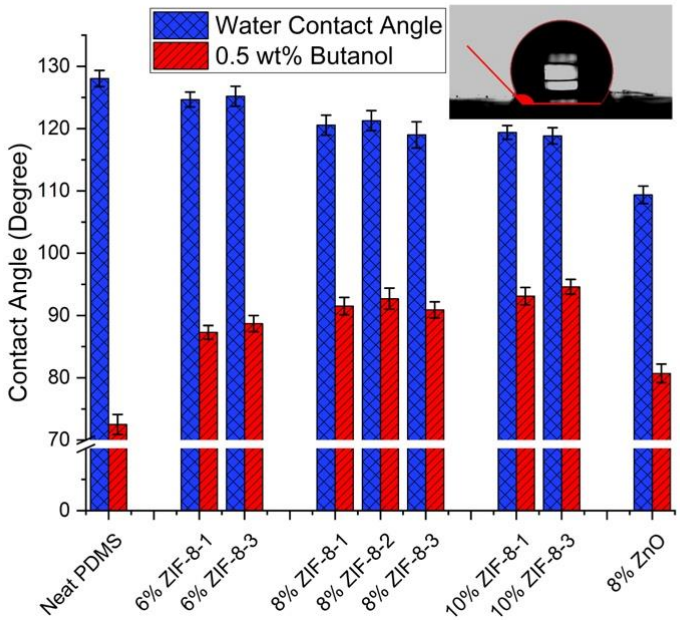

Figure 2.7. Surface static contact angle of PDMS composite membranes for pure water and 0.5 wt% butanol solution.

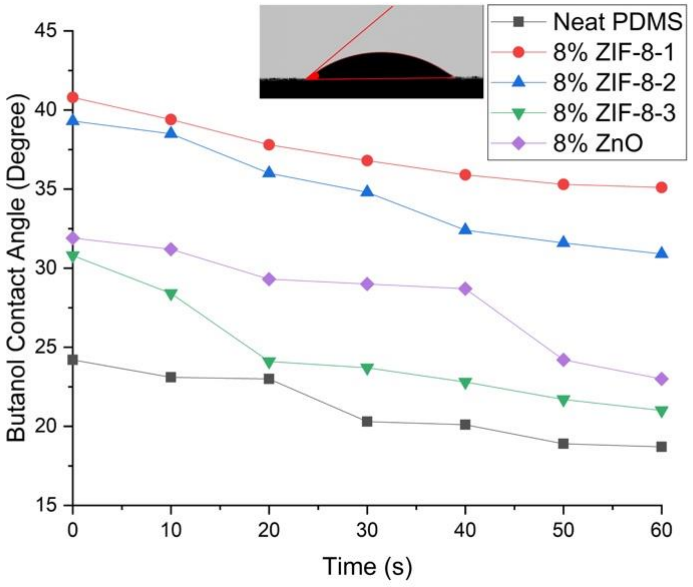

Figure 2.8. Dynamic contact angle of PDMS composite membranes for pure butanol.

2.3.4 Effect of ZIF-8 nanoparticle loading on the membrane performance

The effect of the particle loading on the PV performance of the ZIF-8/PDMS MMMs using 0.5 wt% butanol aqueous solution at 39°C was investigated. For each experiment, three membrane samples were used, and the averaged values of the flux, selectivity and thickness are reported in this section. Very often, the flux and the selectivity are used to assess the membrane pervaporation performance. Results for the total flux and the selectivity for the various MMMs used in this investigation are presented in Figure 2.9. They show that by increasing the ZIF-8-1 loading from 0 to 10 wt%, the total flux increased by 181%, while the selectivity decreased by 72% compared to the neat PDMS membranes. By incorporating porous ZIF-8 into the PDMS polymer chains, the free volume of MMMs increases, accompanied by a decrease in the mass transport resistance, thereby leading to the enhancement of the total flux. Unfortunately, the trade-off between flux and selectivity could not be broken for this particle size.

It is important to note that the flux and the selectivity are not only functions of the inherent properties of the membranes, but also depend on the operating conditions, such as the feed

concentration and temperature, as well as the membrane thickness. Therefore, a better way of reporting the pervaporation data is by normalizing the flux of each component by the feed concentration and the membrane thickness, which in fact defines the membrane permeability P_i as shown in Equation 2.4. These permeability values are shown in Figure 2.10. According to this figure, there was no significant increase in water permeability by adding ZIF-8-1 (larger) particles even though the butanol permeability decreased compared to the neat PDMS membrane. This observation may suggest that the interfacial voids are less likely to affect the membrane performances. It is hypothesized that the PDMS chain mobility may be reduced due to the denser chain packing in the vicinity of the dispersed ZIF-8-1 particles. This phenomenon, known as chain rigidification effect, was investigated for ZIF-8/PDMS membranes by Fang et al. [23]. It is also possible that PDMS chain segments adhere on the surrounding of the pores of ZIF-8 particles and cause pore blockage, which could profoundly impact the permeation of butanol by increasing the membrane diffusion resistance, resulting in low butanol permeability and selectivity. Although there was no overall improvement by embedding ZIF-8-1 (larger) particles compared to the neat PDMS membranes, 8 wt% ZIF-8-1/PDMS membranes showed higher butanol permeability (Figure 2.10) and selectivity (Figure 2.9) than membranes with 6 and 10 wt% loadings. Furthermore, zinc oxide nanoparticles, as non-porous fillers with the same metal core as ZIF-8 but with a very different geometrical shape, was used to illustrate the importance of the particle geometry on the membrane performance. According to Figure 2.9, 8 wt% ZnO/PDMS membranes showed an increase of 811% in the total flux, but at the expense of a 60% decrease in the selectivity in comparison to the pure PDMS membranes. Contrary to the ZIF-8-1 (larger) particles, using non-porous ZnO in the PDMS matrix potentially eliminates the pores blocking effect but increases the possibility of forming interfacial voids between ZnO and PDMS chains due to its complex shape. These voids favour Knudsen diffusion and lead to increased permeance, which supports the increase in the total flux and total permeability observed in Figures 2.9 and 2.10, respectively. On the other hand, these Knudsen dominant voids work as a non-selective pathways that benefit the water molecules, with smaller dynamic diameter than butanol, to diffuse faster and reduce the selectivity dramatically.

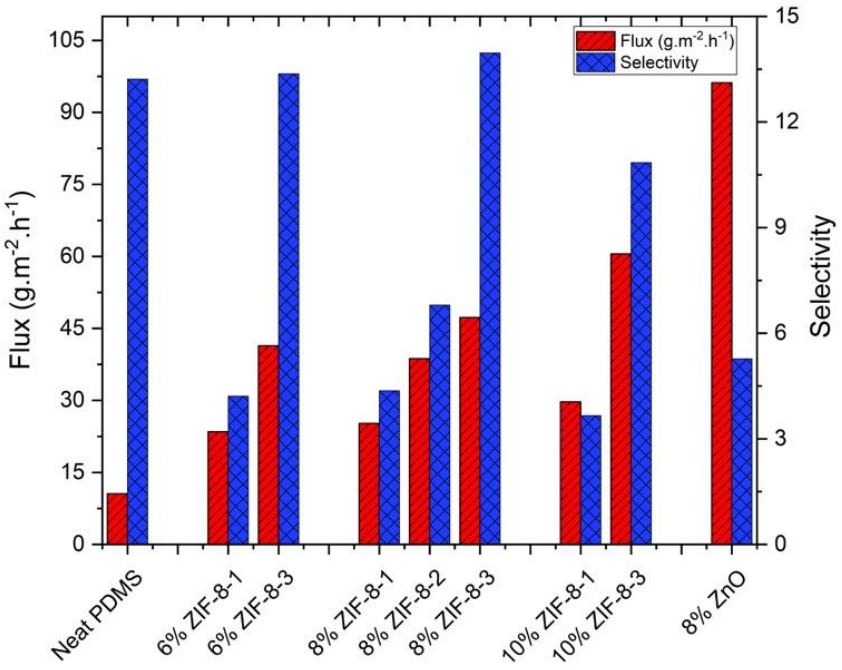

Figure 2.9. Pervaporation separation performance of 0.5 wt% butanol solution for the pure PDMS, ZIF-8/PDMS and ZnO/PDMS membranes at 39°C.

2.3.5 Effect of the ZIF-8 particle sizes on the membrane performance

As previous results suggested, the 8 wt% ZIF-8-1/PDMS membranes presented a better pervaporation performance than MMMs with 6 and 10 wt% loading of ZIF-8-1 nanoparticles. In order to gain a deeper insight with respect to the influence of the filler size on the membrane performance, 8 wt% ZIF-8/PDMS MMMs were fabricated using the smaller particle sizes as ZIF-8-2 and ZIF-8-3 and tested under identical experimental conditions (initial butanol concentration of 5 $g.L^{-1}$, at 39°C). Results presented in Figure 2.9 exhibited a notable difference in MMM permeation performance. Indeed, decreasing the particle size from 80 nm (for ZIF-8-1) to 30 nm (for ZIF-8-3), the total flux and the selectivity increased 88% and 220%, respectively. Increasing both the flux and the selectivity is finally overcoming the trade-off effect associated with the majority PDMS MMMs with enhanced separation performances. Generally, smaller particles provide higher surface area to mass ratio. Therefore, a higher surface area gives a larger

number of active sorption sites and provides an alternative pathway for mass transport through the inner pores of the adsorbent. These pathways act as selective channels in favour of butanol molecules and increase butanol permeability and, as a result, enhanced membrane pervaporation performance. Based on the results of Figure 2.10, the MMM permeability of butanol increased by 59% for the intermediate size ZIF-8-2 nanoparticles and by 252% for the smaller size ZIF-8-3 particles compared to the larger particles 8 wt% ZIF-8-1. Even though butanol permeability significantly increased when the particle size is decreased, the water permeability only increased by 1.8% and 10.2% for MMMs with ZIF-8-2 and ZIF-8-3 nanoparticles compared to MMMs with ZIF-8-1 particles, respectively. However, the surface area is not the only factor affecting the membrane pervaporation performance. As previously mentioned (Section 2.3.4), ZIF-8-1 nanoparticles is supposed to provide similar pathways as ZIF-8-2 and ZIF-8-3. However, it is hypothesized that the ZIF-8-1 nanoparticles may suffer from polymer rigidification and pore blockage. These polymer-particle interactions seem to decrease when smaller particle sizes are used. A study by Yin et al. [24] on ZIF-71 particles with the same Imidazole ligand as ZIF-8 reported that despite the hydrophobicity of ZIF materials, the -N-H group in Imidazole ligand still has a weak hydrophilic character. Therefore, the smaller particles, which have a higher surface area to volume ratio than the larger particles, were thermodynamically driven to agglomerate due to the nature of this hydrophilic surface. Even though particles are evenly dispersed in the polymer matrix and no obvious particle agglomeration was observed, it is highly possible that nano-scale agglomeration occurred. These agglomerated particles have lower interfacial connection with PDMS chains and tend to create voids, instead of pore blocking effect. In this case, ZIF-8/PDMS membranes can actually benefit from voids to overcome pore blocking effects, which can explain the impact of smaller particles on membrane pervaporation performance enhancement. However, if the voids increase significantly by increasing the particle loadings, as 10 wt% ZIF-8-3 membranes in Figure 2.10, the permeability of both water and butanol would increase at the cost of sacrificing the selectivity. Furthermore, both 6 wt% ZIF-8 and 10 wt% ZIF-8/PDMS membranes showed the same behaviour as 8 wt% ZIF-8/PDMS membranes by changing the particle size. The flux increased by adding up to 10 wt% ZIF-8-3 particles to the polymer matrix, but the selectivity only increased up to 8 wt% ZIF-8-3 particle loading, and a sudden decrease is observed at 10 wt%. The best membrane pervaporation separation performance achieved in this study was associated with the 8 wt% ZIF-8-3/PDMS mixed matrix membranes where the flux and the selectivity were

increased up to 350% and 6%, respectively, compared to neat PDMS membranes as can be seen in Figure 2.9.

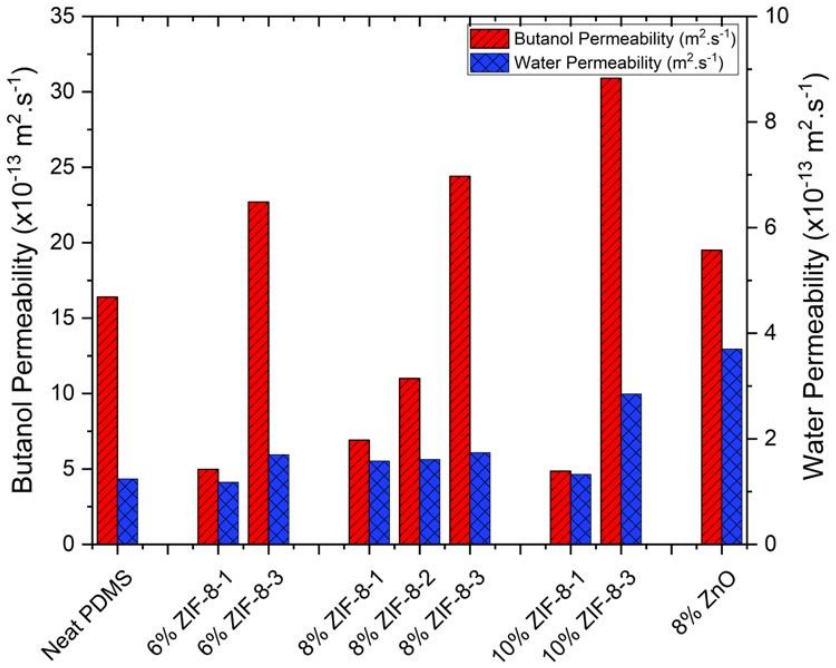

Figure 2.10. Water and butanol permeability for 0.5 wt% butanol solution for the pure PDMS, ZIF-8/PDMS and ZnO/PDMS membranes at 39°C.

2.4 Conclusion

The ultimate goal of this study was to investigate the effect of the filler size on MMM performance for the separation of butanol from aqueous binary solutions, which has been achieved by successful synthesizing different sizes of ZIF-8 nanoparticles (30, 65, and 80 nm) and conducting pervaporation experiments. While butanol permeability, flux and selectivity increased with a decrease in ZIF-8 particle size, water permeability remained constant. Furthermore, ZnO/PDMS membranes were investigated to emphasize the importance of the interface compatibility between filler and polymer chains.

The impact of the ZIF-8 particle loading on the pervaporation separation of butanol from aqueous solution has been studied for three different ZIF-8 sizes. Increase in the ZIF-8 loading content in the MMM with PDMS up to 10 wt% increased the total flux. The maximum selectivity was observed at 8 wt% loading of the small-sized ZIF-8 nanoparticles in the PDMS. The total permeation flux and the butanol selectivity were increased up to 350% and 6%, respectively, for the 8 wt% small-size ZIF-8/PDMS mixed matrix membranes compared to the neat PDMS membrane.

Acknowledgements

Financial support received from NSERC (Natural Sciences and Engineering Research Council) of Canada is gratefully acknowledged.

Abbreviations

ABE	Acetone, Butanol, Ethanol
MOF	Metal organic framework
PAN	Polyacrylonitrile
PDMS	Polydimethylsiloxane
SEM	Scanning Electron Microscope
TEM	Transmission Electron Microscopy
THF	Tetrahydrofuran
XRD	X-ray Powder Diffraction
ZIF	Zeolitic Imidazolate Framework

Nomenclatures

A	Surface area of the membrane (m^2)
$C_{i\text{-feed}}$	Concentration of species *i* in the feed stream ($g.L^{-1}$)

$C_{i\text{-permeate}}$	Concentration of species *i* in the permeate stream ($g.L^{-1}$)
J	Flux ($g.m^{-2}.h^{-1}$)
m_i	Mass of species *i* in the permeate stream (g)
P_i	Membrane permeability of species *i* ($m^2.s^{-1}$)
t	Time of permeation (h)
W_{PDMS}	Weight of the PDMS polymer (g)
$W_{ZIF\text{-}8}$	Weight of the ZIF-8 nanoparticles (g)
x_i	Mass fraction of species *i* in the feed stream ($g_i.g^{-1}_{solution}$)
y_i	Mass fraction of species *i* in the permeate stream ($g_i.g^{-1}_{solution}$)
σ	Membrane effective thickness (μm)
α_i	Selectivity of species *i*

References

[1] N. Qureshi, M.M. Meagher, J. Huang, R.W. Hutkins, Acetone butanol ethanol (ABE) recovery by pervaporation using silicalite-silicone composite membrane from fed-batch reactor of Clostridium acetobutylicum, J. Memb. Sci. (2001). doi:10.1016/S0376-7388(00)00667-0.

[2] S.K. Thangavelu, A.S. Ahmed, F.N. Ani, Review on bioethanol as alternative fuel for spark ignition engines, Renew. Sustain. Energy Rev. 56 (2016) 820–835. doi:10.1016/J.RSER.2015.11.089.

[3] D.C. Rakopoulos, C.D. Rakopoulos, E.G. Giakoumis, A.M. Dimaratos, D.C. Kyritsis, Effects of butanol–diesel fuel blends on the performance and emissions of a high-speed DI diesel engine, Energy Convers. Manag. 51 (2010) 1989–1997. doi:10.1016/J.ENCONMAN.2010.02.032.

[4] T.C. Ezeji, N. Qureshi, H.P. Blaschek, Butanol fermentation research: Upstream and downstream manipulations, Chem. Rec. 4 (2004) 305–314. doi:10.1002/tcr.20023.

[5] T.K. Chua, D.-W. Liang, C. Qi, K.-L. Yang, J. He, Characterization of a butanol–acetone-producing Clostridium strain and identification of its solventogenic genes, Bioresour. Technol. 135 (2013) 372–378. doi:10.1016/J.BIORTECH.2012.08.085.

[6] H. Huang, V. Singh, N. Qureshi, Butanol production from food waste: a novel process for producing sustainable energy and reducing environmental pollution, Biotechnol. Biofuels. 8 (2015) 1–12. doi:10.1186/s13068-015-0332-x.

[7] A. Pugazhendhi, T. Mathimani, S. Varjani, E.R. Rene, G. Kumar, S.H. Kim, V.K. Ponnusamy, J.J. Yoon, Biobutanol as a promising liquid fuel for the future - recent updates and perspectives, Fuel. (2019). doi:10.1016/j.fuel.2019.04.139.

[8] C.H. Park, Q. Geng, Simultaneous fermentation and separation in the ethanol and abe fermentation, Sep. Purif. Rev. 21 (1992) 127–174. doi:10.1080/03602549208021421.

[9] C. Chen, Z. Xiao, X. Tang, H. Cui, J. Zhang, W. Li, C. Ying, Acetone–butanol–ethanol fermentation in a continuous and closed-circulating fermentation system with PDMS membrane bioreactor, Bioresour. Technol. 128 (2013) 246–251. doi:10.1016/J.BIORTECH.2012.10.077.

[10] H. Azimi, A. Ebneyamini, F.H. Tezel, J. Thibault, Separation of organic compounds from ABE model solutions via pervaporation using activated carbon/PDMS mixed matrix membranes, Membranes (Basel). 8 (2018) 1–15. doi:10.3390/membranes8030040.

[11] L.M. Robeson, The upper bound revisited, J. Memb. Sci. 320 (2008) 390–400. doi:10.1016/J.MEMSCI.2008.04.030.

[12] A. Ebneyamini, H. Azimi, F.H. Tezel, J. Thibault, Mixed matrix membranes applications: Development of a resistance-based model, J. Memb. Sci. 543 (2017) 351–360. doi:10.1016/J.MEMSCI.2017.08.065.

[13] P. Shao, A. Kumar, Separation of 1-butanol/2,3-butanediol using ZSM-5 zeolite-filled polydimethylsiloxane membranes, J. Memb. Sci. 339 (2009) 143–150. doi:10.1016/J.MEMSCI.2009.04.042.

[14] H.B. Tanh Jeazet, C. Staudt, C. Janiak, Metal-organic frameworks in mixed-matrix membranes for gas separation, Dalt. Trans. 41 (2012) 14003–14027. doi:10.1039/c2dt31550e.

[15] H. Azimi, F.H. Tezel, J. Thibault, Effect of embedded activated carbon nanoparticles on the performance of polydimethylsiloxane (PDMS) membrane for pervaporation separation of butanol, J. Chem. Technol. Biotechnol. 92 (2017) 2901–2911. doi:10.1002/jctb.5306.

[16] D. Yang, C. Cheng, M. Bao, L. Chen, Y. Bao, C. Xue, The pervaporative membrane with vertically aligned carbon nanotube nanochannel for enhancing butanol recovery, J. Memb. Sci. 577 (2019) 51–59. doi:10.1016/j.memsci.2019.01.032.

[17] G. Liu, Z. Jiang, K. Cao, S. Nair, X. Cheng, J. Zhao, H. Gomaa, H. Wu, F. Pan, Pervaporation performance comparison of hybrid membranes filled with two-dimensional ZIF-L nanosheets and zero-dimensional ZIF-8 nanoparticles, J. Memb. Sci. (2017). doi:10.1016/j.memsci.2016.09.064.

[18] M. Wiebcke, J. Cravillon, S. Münzer, S.J. Lohmeier, A. Feldhoff, K. Huber, S. Münzer, Rapid Room-Temperature Synthesis and Characterization of Nanocrystals of a Prototypical Zeolitic Imidazolate Framework, Chem. Mater. 21 (2009) 1410–1412. doi:10.1021/cm900166h.

[19] K.S. Park, Z. Ni, A.P. Côté, J.Y. Choi, R. Huang, F.J. Uribe-Romo, H.K. Chae, M. O'Keeffe, O.M. Yaghi, Exceptional chemical and thermal stability of zeolitic imidazolate frameworks, Proc. Natl. Acad. Sci. 103 (2006) 10186–10191. doi:10.1073/PNAS.0602439103.

[20] C.M. Zimmerman, A. Singh, W.J. Koros, Tailoring mixed matrix composite membranes for gas separations, J. Memb. Sci. 137 (1997) 145–154. doi:10.1016/S0376-7388(97)00194-4.

[21] N. K. Demir, B. Topuz, L. Yilmaz, H. Kalipcilar, Synthesis of ZIF-8 from recycled mother liquors, Microporous Mesoporous Mater. 198 (2014) 291–300. doi:10.1016/j.micromeso.2014.07.052.

[22] C. Wu, X. Qiao, J. Chen, H. Wang, F. Tan, S. Li, A novel chemical route to prepare ZnO nanoparticles, 60 (2006) 1828–1832. doi:10.1016/j.matlet.2005.12.046.

[23] M. Fang, C. Wu, Z. Yang, T. Wang, Y. Xia, J. Li, ZIF-8/PDMS mixed matrix membranes for propane/nitrogen mixture separation: Experimental result and permeation model validation, J. Memb. Sci. 474 (2015) 103–113. doi:10.1016/j.memsci.2014.09.040.

[24] H. Yin, A. Khosravi, L. O'Connor, A.Q. Tagaban, L. Wilson, B. Houck, Q. Liu, M.L. Lind, Effect of ZIF-71 Particle Size on Free-Standing ZIF-71/PDMS Composite Membrane Performances for Ethanol and 1-Butanol Removal from Water through Pervaporation, Ind. Eng. Chem. Res. 56 (2017) 9167–9176. doi:10.1021/acs.iecr.7b01833.

Chapter 3:

Modeling the molecular permeation through mixed matrix membranes incorporating tubular fillers

Ali Zamani, Jules Thibault, F. Handan Tezel

Department of Chemical and Biological Engineering

University of Ottawa, Ottawa, Ontario, Canada K1N 6N5

Abstract

Membrane-based processes are considered as a promising separation method for many chemical and environmental applications such as pervaporation and gas separations. Numerous types of polymeric membranes have been used for these processes due to their good transport properties, ease of fabrication and relatively low fabrication cost per unit membrane area. However, these types of membranes are suffering from the trade-off between permeability and selectivity. Mixed matrix membranes (MMMs), comprising a filler phase embedded into a polymer matrix, have emerged in an attempt to partly overcome some of the limitations of conventional polymer and inorganic membranes. Among them, membranes incorporating tubular fillers are new nanomaterials having the potential for transcending Robeson's upper bound. The results demonstrated that the exceptionally high transport rates are an outcome of the inherent smoothness of the linear channel of the nanotubes. Aligning nanotubes in the host polymer matrix in the direction of permeation can lead to a significant improvement in membrane permeability. However, while much effort has been devoted to experimentally evaluating nanotube mixed matrix membranes, their modeling is mostly based on early theories for mass transport in composite membranes. In this study, the effective permeability of mixed matrix membranes (MMMs) with tubular fillers has been estimated from the steady-state concentration profile within the membrane, which was calculated by solving numerically the Fick diffusion equation. Using this approach, the effects of various structural parameters, including the tubular filler volume fraction, orientation, length-to-diameter aspect ratio, and permeability ratio were assessed. Enhanced relative permeability were obtained with vertically-aligned nanotubes. The relative permeability increases with the permeability ratio, filler volume fraction and the length-to-diameter aspect ratio. For

water-butanol separation, MMMs using polydimethylsiloxane (PDMS) with nanotubes did not lead to performance enhancement in terms of permeability and selectivity. The results were then compared with analytical prediction models such as Maxwell, Hamilton-Crosser and Kang-Jones-Nair (KJN) models. Overall, this work presents a useful tool for understanding and designing MMMs with tubular fillers.

3.1 Introduction

The use of membranes in separation processes for chemical, petrochemical and environmental applications has significantly increased in recent years. The main advantages of using membranes in industrial separation processes are the much lower energy requirements and the smaller plant footprint compared to conventional separation processes. In addition, given their high stability, efficiency and ease of processing, employing membranes in industrial processes leads to lower environmental impact and cost [1,2]. Polymeric membranes are currently used commercially in separation processes such as pervaporation [3,4] and gas separations [5]. In gas separation processes, cellulose acetate membranes were employed by Cynara, Separex, and GMS to remove carbon dioxide from natural gas by the mid-1980s and further developed by involving Polyimide hollow-fiber membranes [6]. At about the same time, GENERON introduced the first membrane system to separate nitrogen from air using poly(4-methyl-1-pentene) (TPX) membranes. Due to the collaboration of other companies such as Dupont and Air Liquide, over 10 000 similar systems have already been installed worldwide. However, many gas processes such as oxygen separation or pervaporation applications such as alcohol separation and dehydration, still require better membranes to become more commercially viable [2,6].

Improving the separation performances of a membrane-based process at both laboratory and industrial scales depends largely on the chemical, mechanical and permeation properties of the membrane. Even though polymeric membrane materials are continuously improved [7], polymeric membranes mostly suffer from the well-known trade-off between separation factor and permeating flux [4,8]. In an attempt to improve the separation factor and permeating flux of polymeric membranes, many researchers are now directing their effort in developing mixed matrix membranes (MMMs). It has been reported that MMMs, which are made by embedding a proper organic or inorganic filler in the polymer matrix, can combine the advantages of the higher selectivity of the filler particles and the ease of processing of polymers [3,4,9]. Different filler

materials, such as activated carbons [4], carbon nanotubes (CNTs) [10], zeolites [11] and metal-organic frameworks (MOFs) [12], have been incorporated within the matrix of polymers to make MMMs.

Among all types of fillers, nanotubes are considered as emerging nanostructured materials for their potential to enhance the separation performance of membranes for numerous applications. Since the discovery of carbon nanotubes (CNTs), mixed matrix membranes incorporating different single-wall and multi-wall carbon nanotubes [13,14] have shown their potential due to their exceptional transport properties and their physical compatibility with the polymeric membrane. Although the mass transport properties of CNTs are appealing, the ability to mass produce and fabricate defect-free mixed matrix membranes using CNTs is still challenging and limits their applications to large-scale industrial processes. To address these problems, other nanotubes such as titania [15], halloysite nanotubes [16,17], organosilicon [18] and aluminosilicate [19,20] nanotubes have been investigated. Novel techniques have been developed for the synthesis of nanotubes as well as to manipulate their dimension [21,22] and to modify their surface functionality [23,24]. Recent numerical studies on nanotubes have suggested that they possess up to 3 orders of magnitude larger mass transport rates than other materials with similar channel sizes, such as zeolites. The mass transport rates were also found to be considerably larger than the one predicted based on the Knudsen diffusion [25,26]. However, most nanotubes have impermeable side wall such that the orientation of nanotubes does greatly impact on the achievable mass transport as the permeant can only diffuse in the nanotube axial direction [26–28]. Since Skoulidas et al. [29] atomistic simulations on vertically aligned CNTs demonstrated the extremely high transport rate and permeability of light gases, aligning nanotubes within the membrane has received considerable attention for the development of membrane-based separation technologies.

While there are numerous types of nanotubes and polymers available, a rational choice of both phases toward the preparation of MMMs is necessary. Therefore, theoretical predictions of the separation performance from the pure species permeation properties in these MMMs become increasingly valuable. Up to now, different theoretical models have been developed to predict the performance of both ideal and non-ideal MMMs based on their polymer-particle interface morphology [30,31]. Different models include the modified-Maxwell model proposed by

Vu et al. [32], the modified Lewis−Nielsen model [2,31], the modified Pal model [31] as well as the original and modified Felske model [30] have been developed to estimate the effective permeability of non-ideal MMMs. Generally, these models can predict the permeability and the selectivity for the most common MMM morphologies over a large range of filler loading [2]. However, several additional parameters such as particle pore size and distribution, permeability of species in the rigidified or void layer, filler pore blockage ratio as well as the thickness of the non-ideal phase should be taken into account. These parameters are most sensitive to operating conditions and, since there are no reliable methods yet to measure these parameters, their estimation and determination remain a significant challenge [1].

Even though the ideal polymer-particle interface is generally difficult to achieve, the non-ideality can be negligible in some MMMs depending on the particle size and intrinsic properties of polymer and particle materials [1,2]. Numerous analytical models have been developed for estimating the effective permeability of ideal MMMs with spherical or near-spherical fillers such as activated carbons, zeolites or metal-organic frameworks (MOFs) [1,2,8,33]. The Maxwell model [34] is a well-known correlation to predict the effective permeability in terms of the permeability of the dispersed and continuous phases and the filler volume fraction:

$$\frac{P_{eff}}{P_c} = \frac{P_d + (n-1)P_c + (n-1)(P_d - P_c)\phi}{P_d + (n-1)P_c - (P_d - P_c)\phi} \tag{3.1}$$

where P_{eff} is the effective permeability of the mixed matrix membrane, P_c is the permeability of the polymer matrix (continuous phase), P_d is the permeability of the filler (dispersed phase), ϕ is the volume fraction of the filler ($0 \leq \phi \leq 1$), and n is the shape factor of the filler. Considering the original Maxwell model for near-spherical fillers, the shape factor n is taken as $n = 3$.

The Maxwell correlation can predict the effective permeability of MMMs for spherical and near-spherical fillers fairly accurately up to intermediate filler volume fraction [1]. However, the Maxwell correlation is not well adapted for predicting the effective permeability of particles that deviate significantly from traditional geometry such as for MMMs incorporating tubular fillers as it is difficult to specify the shape factor. A modified Maxwell model, also known as the Hamilton-Crosser model [35], was suggested for the prediction of the effective permeability by substituting the semi-empirical shape factor in the Maxwell equation using Equations (3.2) and (3.3).

$$n = 3\psi^{-g} \tag{3.2}$$

$$\psi = 2 \times \left(\frac{3}{4}\right)^{2/3} \frac{d_o L^2}{d_o + 2L} \tag{3.3}$$

where ψ represents the sphericity of nanotubes, g is an empirical parameter taken as $g = 1$, L and d_o are the length and outer diameter of the nanotubes, respectively. Although the Hamilton-Crosser model can estimate permeation in composite membranes containing nanotubes by using a shape factor, the assumption that the fillers have an isotropic permeability makes it inconsistent with the high mass transport in the axial direction of the nanotubes. Furthermore, the Hamilton-Crosser model assumes that the fillers are randomly oriented, whereas nanotubes could be well aligned in the mixed matrix membranes [10].

The Kang-Jones-Nair (KJN) model [26] is among the few analytical models that were proposed to estimate the effective permeability considering the orientation of the nanotubes and their permeability in the axial direction (Equations (3.4)-(3.6)).

$$\frac{P_{eff}}{P_c} = \left[\left(1 - \frac{\cos(\theta)}{\cos(\theta) + \frac{1}{\alpha}\sin(\theta)}\phi\right) + \frac{P_c}{P_d}\left(\frac{1}{\cos(\theta) + \frac{1}{\alpha}\sin(\theta)}\right)\phi\right]^{-1} \tag{3.4}$$

$$\phi = \frac{V_d}{V_t} \tag{3.5}$$

$$\alpha = \frac{L}{d_o} \tag{3.6}$$

where P_{eff} is the effective permeability of the mixed matrix membrane, P_c is the permeability of the continuous phase, P_d is the permeability of the dispersed phase, ϕ is the volume fraction of the filler ($0 \leq \phi \leq 1$), V_t is the total volume, V_d is the dispersed phase volume based in the length and outside diameter of the nanotube, θ is the orientation with respect to the axis parallel to the main migration direction and nanotube aspect ratio α which is the length (L) over the outer diameter (d_o) ratio.

Even though the KJN model can account for the orientation and aspect ratio of the nanotubes, a one-dimensional (1D) mass transfer was assumed for its derivation. This approximation may not represent adequately the three-dimensional (3D) mass transport phenomena occurring in MMMs and consequently reduces the reliability of the KJN model. In addition, the KJN model cannot be used for completely impermeable filler particles.

To assess the degree of accuracy of the previously-mentioned models for the estimation of the effective permeability, the three-dimensional Fick's equation was solved numerically to determine the steady-state permeation flux of a mixed matrix membrane containing nanotubes. The steady-state permeation flux allows to calculate, for a given MMM, its effective permeability. The numerical investigation allows to study the effects of the filler orientation, the length-to-diameter aspect ratio, and the permeability ratio between the continuous and dispersed phases on the effective permeability. The results were compared with the Maxwell, Hamilton-Crosser and the KJN models and provided data to potentially develop a better predictive model.

3.2 Computational methods

3.2.1 Mixed matrix membrane model construction

Assuming a homogenous dispersion of the filler particles with the same orientation within the polymeric membrane, as shown in Figure 3.1(a), a mixed matrix membrane can be described as the repetition of a unit element. Each unit element has an identical effective permeability, which gives an accurate representation of the permeability of the entire mixed matrix membrane. Hence, it is possible to solve numerically for a unique unit element, as shown in Figure 3.1, to determine the effective permeability of the MMM. Figure 3.1**(**b) shows that each repeatable unit of the mixed matrix membrane, which has been referred to as a "unit element" in this work, has three distinct regions: (1) the polymeric continuous phase surrounding the filler, (2) the hollow cylindrical filler particle located in the center of the unit and (3) the cylindrical void phase inside the filler.

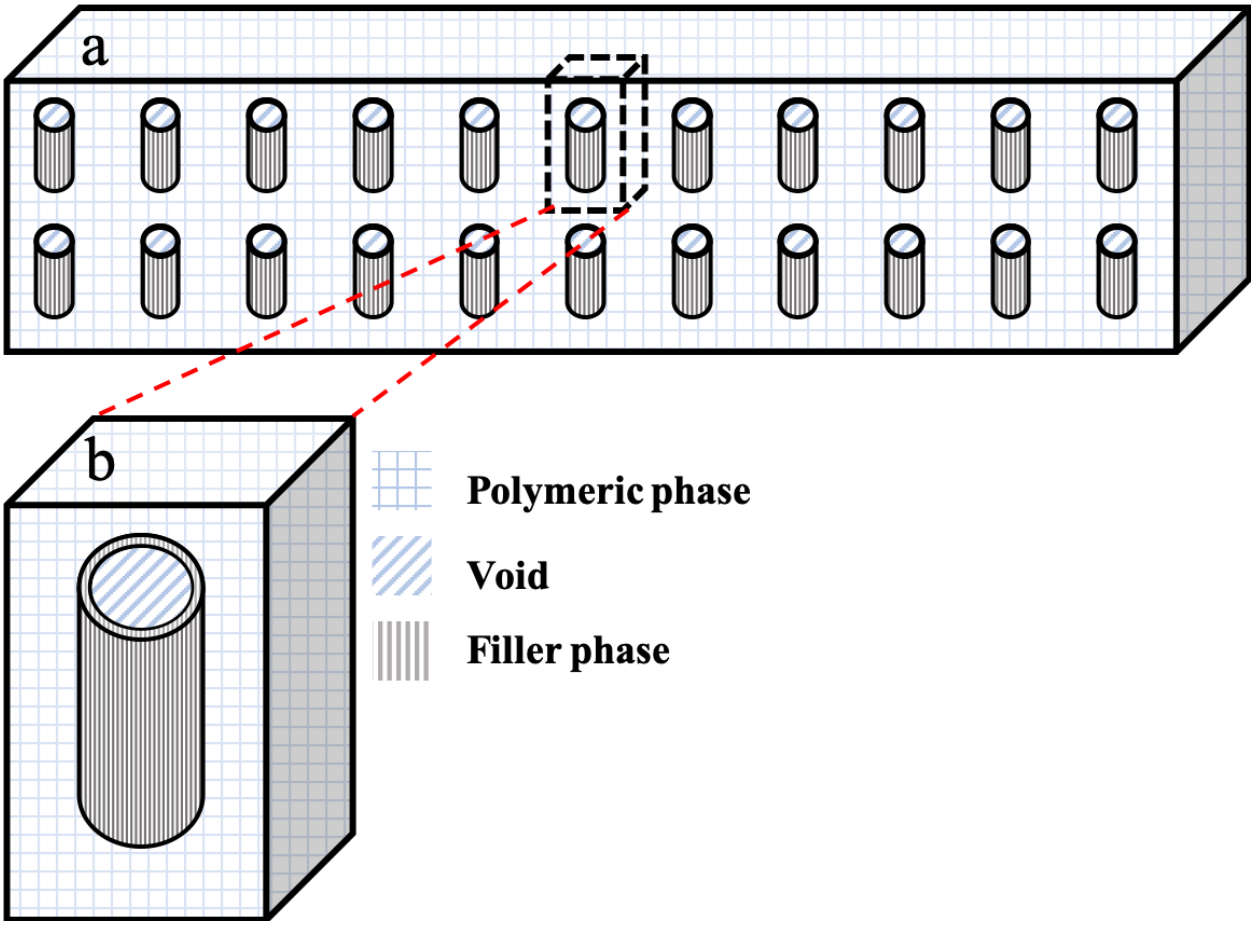

Figure 3.1. a) A schematic diagram of the cross-section of a homogenous dispersed nanotube particles in a mixed matrix membrane, **b)** Schematic diagram of a repetitive unit element including the polymer and filler phases as well as void volume inside the nanotube.

3.2.2 Modeling mass transfer

The three-dimensional Fick's second law of diffusion (Equation (3.7)) was solved numerically for all phases to determine the concentration profile within MMMs as a function of time and under steady-state:

$$\frac{\partial C}{\partial t} = \frac{\partial}{\partial x}\left(D_{x,y,z}\frac{\partial C}{\partial x}\right) + \frac{\partial}{\partial y}\left(D_{x,y,z}\frac{\partial C}{\partial y}\right) + \frac{\partial}{\partial z}\left(D_{x,y,z}\frac{\partial C}{\partial z}\right) \qquad (3.7)$$

where C is the concentration, D is the diffusion coefficient in x, y and z directions and t is the time.

In this investigation, it was assumed that the particle-filler interface morphology was ideal, and the concentration of the feed solution in contact with the retentate side of the membrane remains constant while perfect vacuum prevails on the permeate side. Constant solubility (*S*) of the migrating species and instantaneous equilibrium are assumed at the fluid-membrane interface. Since it is assumed that the membrane is made of a large number of identical unit elements, periodic boundary conditions (PDC) exist at the four faces parallel to the main permeation direction. Considering that it is the steady-state permeation flux that is of interest in order to calculate the effective permeability, a linear concentration profile in the main permeation direction was used as the initial condition for the concentration profile in order to reduce the convergence time required to achieve steady-state. It is important to note that the final steady-state concentration profile and permeate flux are independent of the initial conditions. The initial and boundary conditions for the mass transfer simulations used in this investigation are summarized in Table 3.1.

Table 3.1. Initial and boundary conditions used in all simulations.

Initial Condition	
$At\ t = 0$	$C_{(x,y,z)}\big\vert_{t=0} = C_{(x,0,z)} - \dfrac{C_{(x,0,z)} - C_{(x,L_2,z)}}{N_y - 1}$
Boundary Conditions	
$At\ y = 0$	$C_{(x,0,z)} = C_f . S_{(x,0,z)}$
$At\ y = L_2$	$C_{(x,L_2,z)} = 0$
$At\ x = 0\ and\ x = L_1$	$\dfrac{\partial C}{\partial x}\Big\vert_{x=0} = \dfrac{\partial C}{\partial x}\Big\vert_{x=L_1} = 0$
$At\ z = 0\ and\ z = L_3$	$\dfrac{\partial C}{\partial z}\Big\vert_{z=0} = \dfrac{\partial C}{\partial z}\Big\vert_{z=L_3} = 0$

3.2.3 Numerical methods and solution post-processing

The three-dimensional dynamic and steady-state concentration distributions within one repeatable unit element of a MMM were obtained by solving numerically the Fick's diffusion equation (Equation (3.7)) using the finite differences method (FD). The computer code to solve the Fick's diffusion equation was written in FORTRAN. The unit element consists of a finite hollow cylindrical filler located at the center of a rectangular cuboid. The unit element was discretized into a sufficiently large number of mesh points by implementing OpenFOAM software to generate

small cubical elements, each consisting of only one phase (continuous or dispersed phase). The dimensions of the unit element and the filler as well as the discretization mesh size were kept constant. In some cases, the number of filler particles embedded in the unit element was varied from 0 to 4 in order to calculate the concentration profile for different volume fractions of the dispersed phase. For all numerical simulations, the largest possible mesh size was selected for which the mesh independency prevailed in order to obtain at the same time an accurate solution and lower computation time.

Assuming that the solubility and mass diffusivity of each permeating species remained constant throughout the unit element and the membrane, Equation (3.8) was used to calculate the concentration of each species (m) at mesh point (i, j, k) at the next time step $t + \Delta t$.

$$C_{i,j,k}^{m,t+\Delta t} = C_{i,j,k}^{m,t} + \Delta t \begin{bmatrix} -D_{i,j,k}^{LX} \dfrac{(C_{i,j,k}^{m,t} - \dfrac{S_{i,j,k}}{S_{i-1,j,k}} C_{i-1,j,k}^{m,t})}{\Delta x^2} & +D_{i,j,k}^{RX} \dfrac{(\dfrac{S_{i,j,k}}{S_{i+1,j,k}} C_{i+1,j,k}^{m,t} - C_{i,j,k}^{m,t})}{\Delta x^2} \\ -D_{i,j,k}^{LY} \dfrac{(C_{i,j,k}^{m,t} - \dfrac{S_{i,j,k}}{S_{i,j-1,k}} C_{i,j-1,k}^{m,t})}{\Delta y^2} & +D_{i,j,k}^{RY} \dfrac{(\dfrac{S_{i,j,k}}{S_{i,j+1,k}} C_{i,j+1,k}^{m,t} - C_{i,j,k}^{m,t})}{\Delta y^2} \\ -D_{i,j,k}^{LZ} \dfrac{(C_{i,j,k}^{m,t} - \dfrac{S_{i,j,k}}{S_{i,j,k-1}} C_{i,j,k-1}^{m,t})}{\Delta z^2} & +D_{i,j,k}^{RZ} \dfrac{(\dfrac{S_{i,j,k}}{S_{i,j,k+1}} C_{i,j,k+1}^{m,t} - C_{i,j,k}^{m,t})}{\Delta z^2} \end{bmatrix} \quad (3.8)$$

The concentration change at mesh point (i, j, k) during the time interval Δt only depends on the current concentration at the mesh point and the six neighbouring mesh points at time t. Since the dispersed and continuous phases have different properties, the solubility of each phase is different. Therefore, the solubility ratio of each neighbouring mesh points used to convert all the concentrations to the same phase basis as the phase of the center mesh point (i, j, k). A mass balance in x, y and z directions were performed to calculate the effective diffusivity coefficient of each mesh point within the matrix of the membrane due to their solubility and diffusivity difference. Equations (3.9) and (3.10) give the equations that were used to calculate the effective diffusivity in the x-direction between mesh point (i, j, k) and its left (L) neighbour (i-1, j, k), and between mesh point (i, j, k) and its right (R) neighbour (i+1, j, k), respectively. Similar equations were derived for the effective diffusion coefficients in the other two dimensions and were substituted in Equation (3.8).

$$\frac{1}{D_{i,j,k}^{LX}} = \frac{S_{i,j,k}}{S_{i-1,j,k}} \frac{1}{2D_{i-1,j,k}} + \frac{1}{D_{i,j,k}} \tag{3.9}$$

$$\frac{1}{D_{i,j,k}^{RX}} = \frac{S_{i,j,k}}{S_{i+1,j,k}} \frac{1}{2D_{i+1,j,k}} + \frac{1}{D_{i,j,k}} \tag{3.10}$$

The Fick's first law of diffusion, given in Equation (3.11), was used to estimate the average permeation flux of a permeant at the permeate side of the membrane based on all surface mesh points of the x-z plane (Equation (3.12)). A similar equation was used for estimating the permeation flux at the feed side of the membrane.

$$J_{(i,N_y,k)} = -D_{x,y,z} \left.\frac{\partial C}{\partial y}\right|_{y=L_2} \tag{3.11}$$

$$J_m|_{y=L_2} = \sum_{i=1}^{N_x} \sum_{k=1}^{N_z} \frac{\omega_i \omega_k J_{(i,N_y,k)}}{(N_x-1)(N_z-1)} with \quad \omega_i = \begin{cases} 0.5, i = 1 \; or \; N_i \\ 1, i \in [2, N_x - 1] \end{cases} \quad \omega_k = \begin{cases} 0.5, k = 1 \; or \; N_z \\ 1, k \in [2, N_z - 1] \end{cases} \tag{3.12}$$

where J_m is the average permeation flux of component *m* calculated for a *x*-*z* plane. N_x, N_y and N_z are the number of mesh points used to discretize Equation (3.7) in the *x*, *y* and *z* directions, respectively. Given the estimation of the permeation flux, the concentration difference across the unit element and the thickness of the unit element, the effective permeability of a permeant in a MMM can be calculated using Equation (3.13).

$$P_{m,eff} = \frac{J_m . L_2}{C_{m,f} - C_{m,p}} \tag{3.13}$$

where L_2 is the thickness of the unit element, $C_{m,f}$ and $C_{m,p}$ are the concentrations of component *m* in the feed and permeate side, respectively.

It is important to note that the simulations were run until the difference between the permeation fluxes at the feed and the permeate side of the membrane achieved a relative error smaller than 0.01% to ensure steady-state conditions prevailed. As illustrated in Figure 3.2, the tubular filler is described by an inner diameter (d_i), a length-to-outside diameter aspect ratio (α) calculated using Equation (3.6), and orientation defined by an angle θ (varying from 0 to 90 degrees) with

respect to the axis parallel to the main migration direction (y-direction). The diffusion coefficient and solubility factor for the continuous polymer phase were varied for different case studies while the permeation mechanism inside the nanotube was assumed to follow Knudsen diffusion. As a result, the permeability of the nanotube channel (dispersed phase) was estimated using Equation (3.14).

$$P_d = S_d D_d = \frac{1}{RT}\sqrt{\frac{8{d_i}^2 RT}{9\pi M}} \tag{3.14}$$

where, D_d is the Knudsen diffusivity, S_d is the solubility factor, d_i is the inner diameter of the nanotube, and M is the molecular weight of the transported molecule.

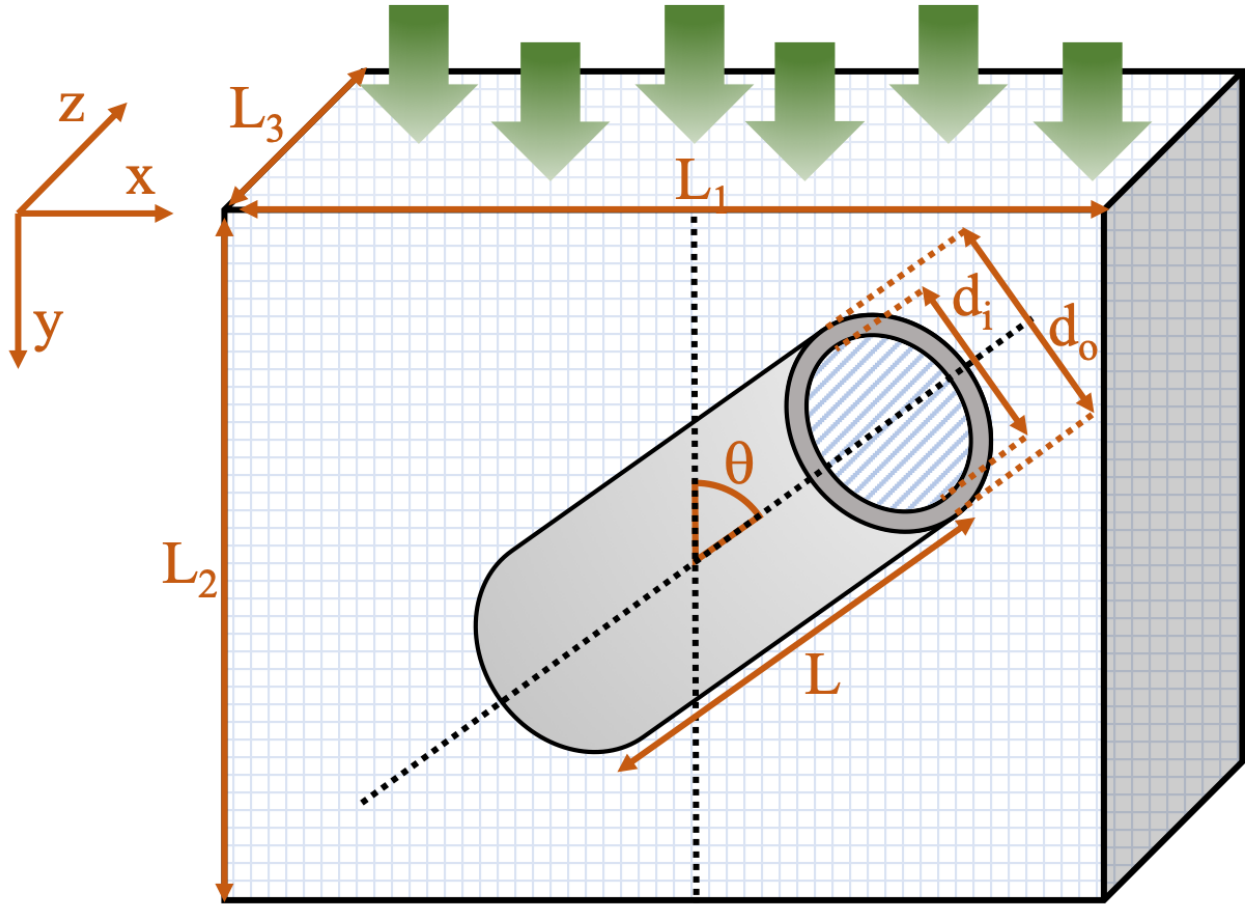

Figure 3.2. Schematic diagram of a repetitive unit element of a MMM.

3.3 Results and discussion

3.3.1 Unit element validation

In this section, four different numerical simulation studies were performed to show unequivocally that the effective permeability of a repeatable unit of a MMM is identical to the effective permeability of the whole mixed matrix membrane with similarly-aligned and uniformly distributed nanotubes. In Case I (Figure 3.3(b)), a slice of the membrane including four identical unit elements with a nanotube located at their respective center was simulated and the effective permeability of the four unit elements was calculated at steady-state. The four unit elements of Case I was then divided into two slices comprised of two unit elements, a horizontal and a vertical slice represented as Cases II (Figure 3.3(c)) and III (Figure 3.3(d)), respectively. Finally, Case IV (Figure 3.3(e)) considers the typical unit element containing a single filler particle used throughout this investigation. For all case studies, simulations were performed for an aspect ratio of $\alpha = 10$ and a ratio of the permeability of the dispersed phase over the permeability of the continuous phase of $P_d/P_c = 100$ with all tubular fillers oriented along the y-axis and with no species diffusion through the outside wall of the nanotubes. The volume fraction for each case was either 0.1 or 0.4 and was calculated using Equation (3.5). To keep the generality of the results, the effective permeability was reported for each case study as the relative permeability (P_r) as calculated using Equation (3.15).

$$P_r = \frac{P_{eff}}{P_c} \tag{3.15}$$

where P_{eff} and P_c represent the effective permeability of the MMM and the permeability of the continuous phase, respectively. All specifications of the dispersed and continuous phases are summarized in Table 3.2.

Considering the results obtained from the eight numerical simulations of Figures 3.3(b)-3.3(e) and Table 3.2, different cases with different dimensions and spatial distribution yield identical relative permeability. Furthermore, the same results were obtained by performing eight additional simulations with a volume fraction of 0.2 and 0.3. Therefore, each case led to an identical and accurate estimation of the permeability of the entire mixed matrix membrane. However, as shown in Figure 3.4, the computational time increased dramatically by increasing the simulation

dimensions for Cases I, II and III. Thus, Case IV was chosen to pursue for rest of the case studies in this investigation.

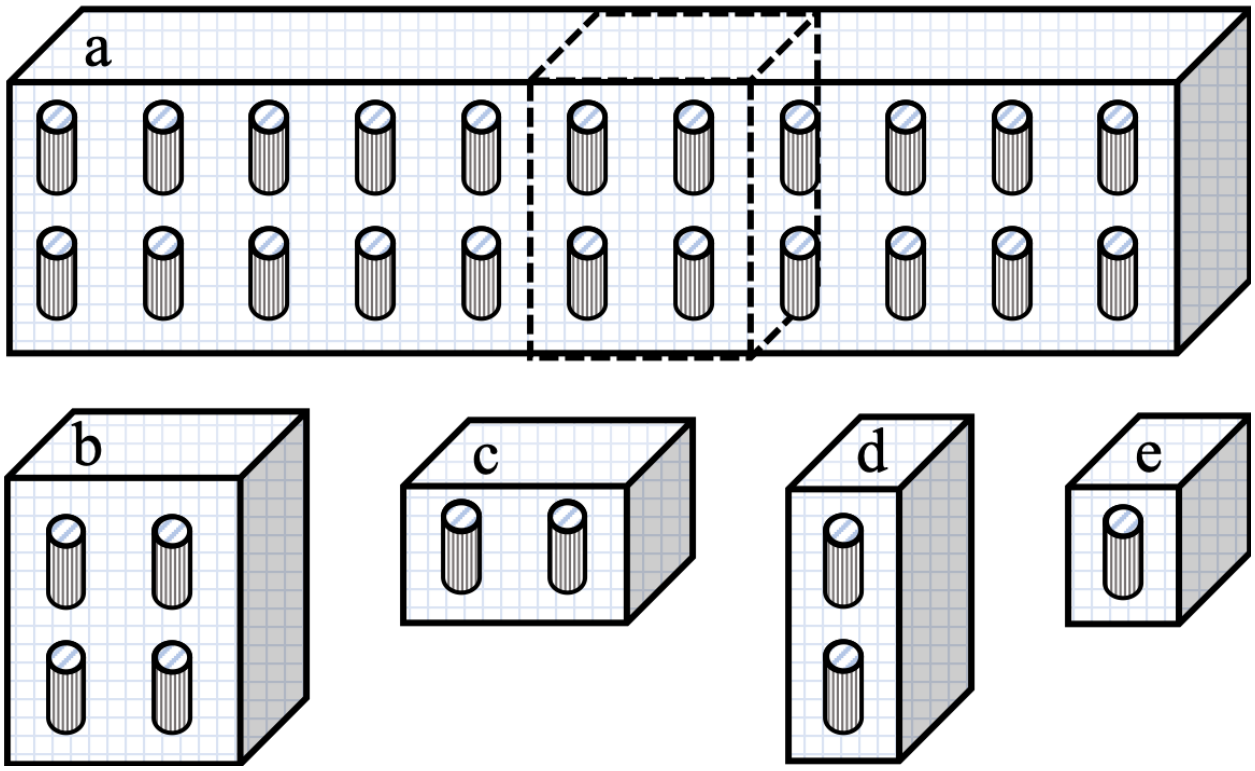

Figure 3.3. a) A schematic diagram of a cross-section of the MMM showing a series of repeatable unit elements. A series of smaller membrane cross-sections: **b)** four unit elements with vertical nanotubes (Case I), **c)** two unit elements with vertical nanotubes distributed in x-axis (Case II), **d**) two unit elements with vertical nanotubes distributed in y-axis (Case III) and **e)** one unit element with a vertical nanotube at the center of the element (Case IV).

Table 3.2. Dispersed and continuous phase specifications

Case	ϕ	Number of unit elements	Simulation dimension $L_1 \times L_2 \times L_3$ (nm)	α	$d_o(nm)$	$d_i(nm)$	$\frac{P_d}{P_c}$
I	0.1	4	$10.6 \times 44 \times 5.3$	10	2.0	0.8	100
	0.4		$5.4 \times 44 \times 2.7$				
II	0.1	2	$10.6 \times 22 \times 5.3$				
	0.4		$5.4 \times 22 \times 2.7$				
III	0.1	2	$5.3 \times 44 \times 5.3$				
	0.4		$2.7 \times 44 \times 2.7$				
IV	0.1	1	$5.3 \times 22 \times 5.3$				
	0.4		$2.7 \times 22 \times 2.7$				

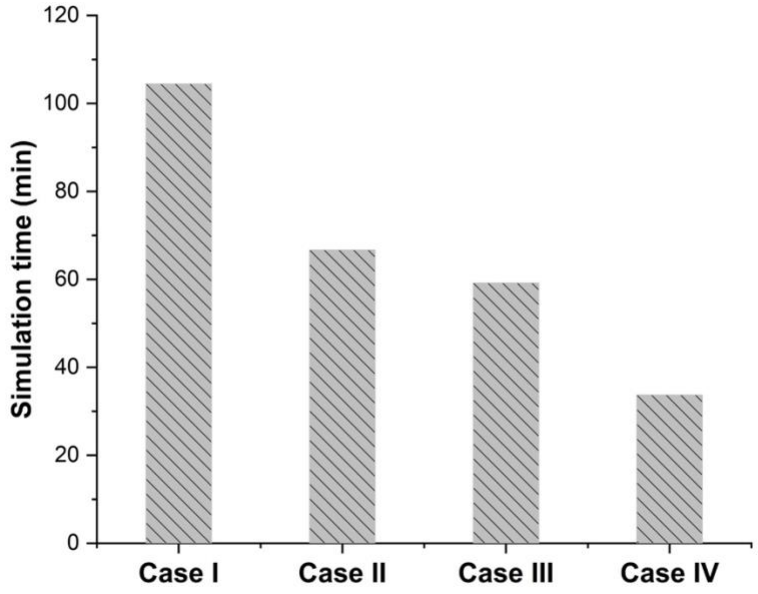

Figure 3.4. Computation times of the numerical simulations for the four different case studies using one core and 1 Gb Ram on the Frontenac cluster nodes available at Centre for Advanced Computing (CAC) at Queens University (Canada).

3.3.2 Effect of the filler orientation on the effective permeability

Recent research on the use of nanotubes as a filler in MMMs is generally focused on incorporating different types of nanotubes in different polymer matrices in order to achieve a higher effective permeability. Usually, these mixed matrix membranes are fabricated by incorporating nanotubes without applying an external driving force to align the nanotubes with a preferred orientation. However, the possibility of controlling the filler orientation in mixed matrix membranes is what makes the nanotube fillers more advantageous over other types of nano-porous materials.

As clearly shown by Ebneyamini et al. [8], the effective permeability of the membrane for a permeant depends on the permeability of each phase and not on the individual values of the solubility factor and diffusion coefficient but rather on the product of the two. Therefore, to investigate the effect of the orientation of the nanotubes, five numerical simulations of a unit element incorporating a single nanotube with different filler orientations were performed. The five angles tested were 0, 30, 45, 60 and 90 degrees, the permeability ratio of the dispersed phase and the continuous phase was kept constant at a value of $P_d/P_c = 100$, and the length-to-diameter ratio α was set to 10. Results on the effect of the nanotube orientation in terms of the relative permeability (P_{eff}/P_c) are presented in Figure 3.5 for three different filler volume fractions. As expected, the results of Figure 3.5 show that a higher filler volume fraction has the larger effect on the relative permeability. The vertical orientation of high permeability nanotubes provides a longer projected preferential permeation pathway for the molecules to diffuse across the membrane, thereby enhancing the relative permeability of the membrane. Even though the vertical filler provides smaller surface of higher permeability relative to the impermeable area between the inner and the outer diameter, the effective permeability of the membrane was significantly increased due to the high permeability in the axial direction of the filler. On the other hand, the horizontal orientation presents the lowest effective permeability. As previously mentioned, there is no mass diffusion occurring through the side wall of nanotubes, so molecular species must contour these impermeable walls to migrate through the membrane. Consequently, the side wall acts as an additional mass transfer resistance that increases by increasing the filler angle from 0_o to 90_o. The maximum resistance occurs at a horizontal orientation where these fillers act as barrier material. Results in Figure 3.5 show that the enhancement and reduction in the effective permeability were magnified by increasing the filler volume fraction. For this particular case study, at an angle in the

vicinity of 45°, results show that the enhancement and the reduction in the effective permeability cancel each other. It is therefore obviously desirable to align the nanotubes in the direction of permeation of the molecular species.

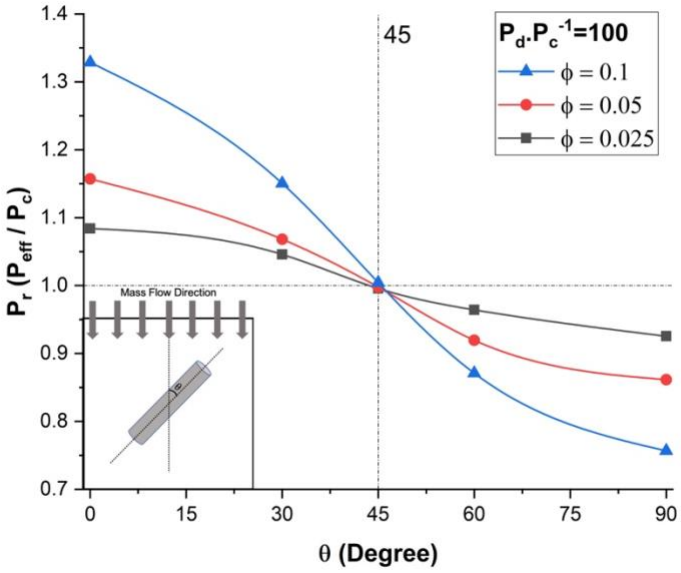

Figure 3.5. Relative permeability for different nanotubes orientations and volume fractions at $P_d.P_{c-1}$=100 and α = 10.

3.3.3 Effect of the permeability ratio of the nanotubes on the effective permeability

To assess the effect of the dispersed-to-continuous phase permeability ratio (P_d/P_c) on the relative permeability P_r of mixed matrix membranes incorporating nanotubes, a series of numerical simulations were performed for five different nanotube orientations and three filler volume fractions. For all simulations, the length-to-diameter aspect ratio α of the nanotube and the outside-to-inside diameter ratio of the diameter d_0/d_i were 10 and 2.5, respectively. Results for five different permeability ratios (P_d/P_c) from 0 to 1000 are presented in Figure 3.6.

Results of Figure 3.6 show that the relative permeability P_r of the mixed matrix membrane increased with an increase of the dispersed-to-continuous phase permeability ratio. As observed in

the previous section, this permeability improvement is highly dependent on the nanotube orientation and a higher relative permeability is obtained with nanotubes oriented in the direction of species permeation ($\theta = 0_o$). For a permeability ratio (P_d/P_c) of 1000, the relative permeability increased by 43% for vertically-aligned nanotubes and a volume fraction of 0.10. The permeability along the axial direction of the nanotubes provides a preferential diffusion pathway for the permeating species to migrate more rapidly. Further increasing the permeability ratio will not lead to a higher relative permeability because the species still have to migrate through the less permeable polymer section before reaching the nanotubes and the polymer matrix becomes the limiting factor in the effective permeability.

Results of Figure 3.6 highlight a very interesting phenomenon regarding the range of angles of nanotubes for which the relative permeability P_r is above unity, which is completely independent of the volume fraction and the intersection point with the relative permeability of unity could be referred as the break-even point. These results show that nanotubes enhance the effective permeability of the membrane when the orientation of the nanotubes are above the break-even point. For very high permeability ratio (P_d/P_c), there exists an improvement in the effective permeability of the mixed matrix membrane for angles up to roughly 50_o and the angle for the break-even point decreases as the permeability ratio decreases. The angle is only 10_o when the permeability ratio (P_d/P_c) is equal to 10. The enhancement completely disappears at a permeability ratio in the vicinity of 5. Above the angle for the break-even point, the nanotubes act as a barrier material due to the impermeability of the nanotube wall. For a permeability ratio (P_d/P_c) of unity and vertically-aligned nanotubes, the relative permeability is below one because of the volume fraction occupied by the impermeable walls of the nanotubes, which offer an additional resistance to mass transfer.

At $P_d/P_c=0$, the filler assumed to be a non-porous cylinder. Figure 3.6 acknowledges the fact that there is no significant difference in effective permeability between $P_d/P_c=1$ and $P_d/P_c=0$. The relative permeability P_r in both cases are dependent to the orientation θ and the filler volume fraction, but it is always less than unity. Therefore, nanotube fillers with lower permeability ratio are not suitable if high permeable membranes are desired.

To more clearly visualize the break-even point, the MMM relative permeability P_r was plotted as a function of the orientation of the nanotubes for the five permeability ratios (P_d/P_c) and for

a constant filler volume fraction of 0.10 (Figure 3.7). It is clear that for a permeability ratio of 10 or lower, the use of nanotube fillers even if they are perfectly aligned vertically would not enhance the effective permeability of the membrane. One could argue that for a permeability ratio of unity, the relative permeability should be also unity. However, the volume occupied by the impermeable walls of the nanotubes act as a barrier material and the relative permeability will always be below unity. At an angle θ of 90° (horizontal orientation), the relative permeability of the MMM becomes independent of the dispersed-to-continuous phase permeability ratio (P_d/P_c) as the nanotubes act strictly as barrier materials and there is no diffusion along the axial direction of the nanotubes.

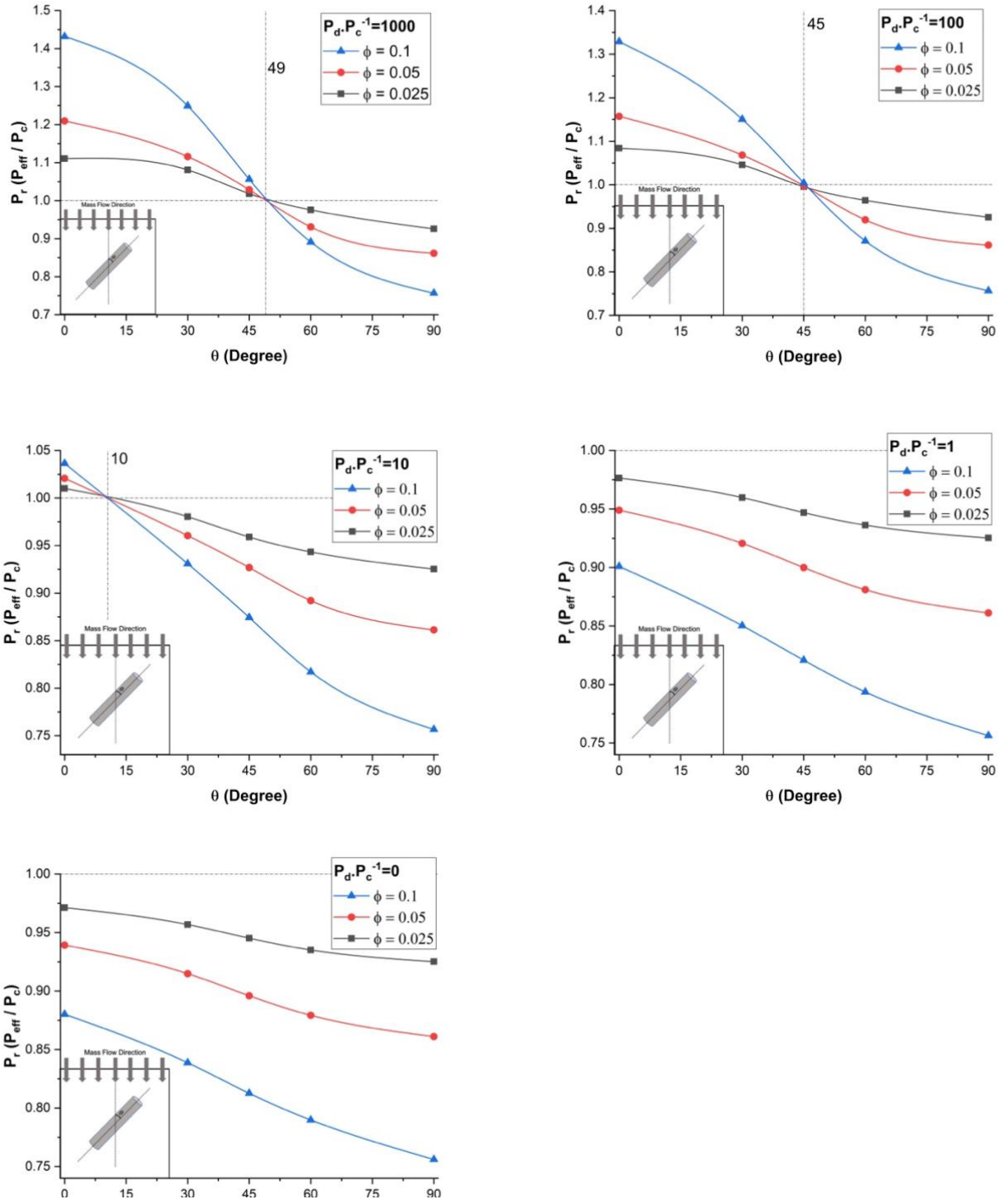

Figure 3.6. Plots of the relative permeability of mixed matrix membranes incorporating nanotubes as a function of the nanotube orientation for five different $P_d.P_{c-1}$ ratios, three filler volume fractions and at a constant length-to-diameter aspect ratio α = 10.

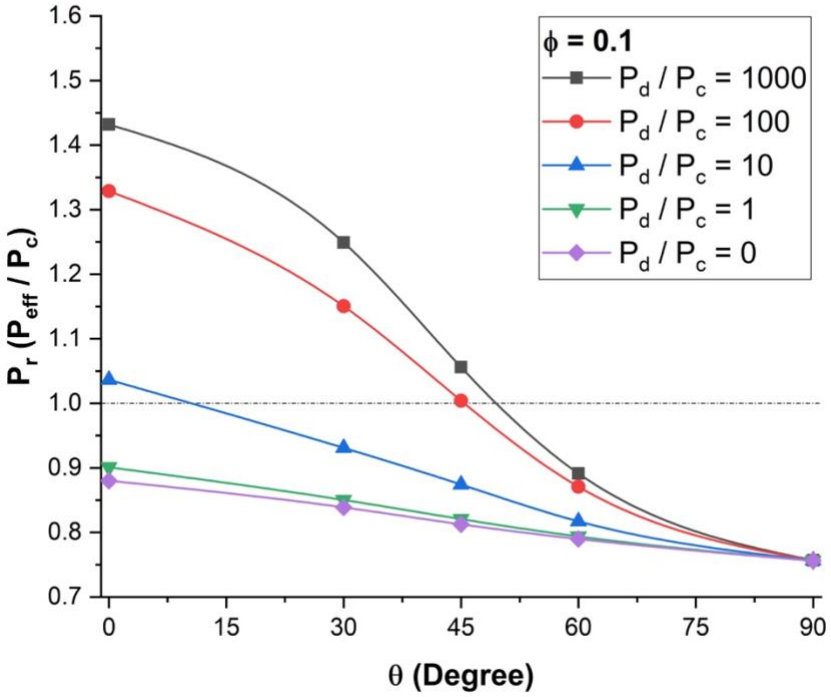

Figure 3.7. Relative permeability for different dispersed-to-continuous permeability ratios $P_d.P_{c-1}$ at a constant volume fraction ϕ = 0.1 and a constant length-to-diameter aspect ratio α = 10.

3.3.4 Effect of the filler aspect ratio of nanotubes on the relative permeability

To investigate the impact of the length-to-diameter aspect ratio (α) of the nanotubes on the relative permeability of MMMs, a series of numerical simulations were performed for five aspect ratios varying from 0 to 100 and various filler volume fractions while the permeability ratio (P_d/P_c) and the orientation were kept constant at 100 and 0_o, respectively. Figure 3.8 presents the plots of the relative permeability of MMMs as a function of the filler volume fraction. For each simulation, the diameter of the nanotubes was kept constant while the filler length was varied. These results clearly show that, with the same filler volume fraction, the effective permeability of MMMs is higher for higher aspect ratios. Similar to the results of previous sections, as expected, increasing the filler volume fraction enhanced the effective permeability for all aspect ratios. These results

indicated that tubular fillers with higher aspect ratios and vertically-aligned nanotubes are preferred for enhancing the effective permeability of MMMs.

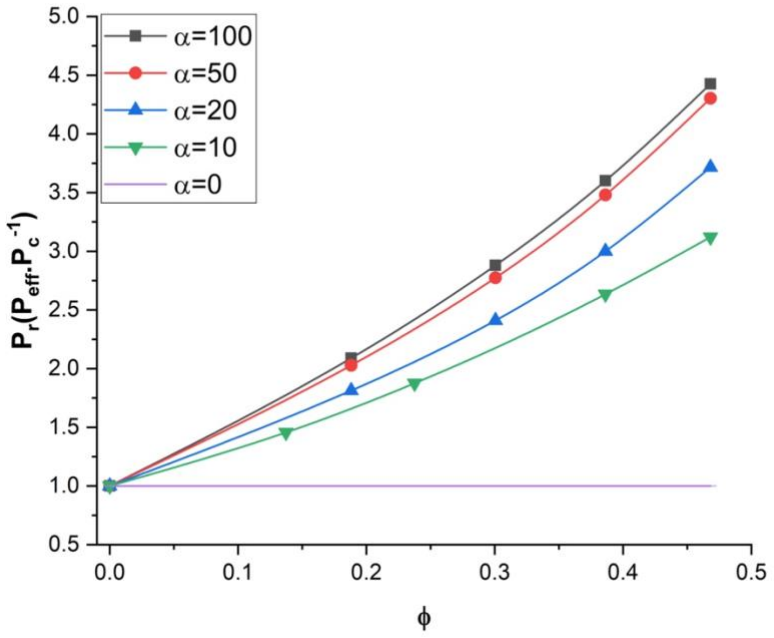

Figure 3.8. Relative permeability for nanotubes with different length-to-diameter aspect ratios at a permeability ratio $P_d.P_{c-1}$ of 100 and an angle θ of 0o.

3.3.5 Separation properties prediction of binary mixtures

The ultimate objective of using mixed matrix membranes is to enhance the separation factor of gas or liquid mixtures. In this investigation, it was desired to examine how a mixed matrix membrane with nanotube fillers could be used for the binary mixture separation of butanol and water. Separation of alcohol/water mixtures using a pervaporation is one of the most popular applications in this field. In this section, a butanol/water binary mixture was chosen to investigate the effect of the nanotube orientation on the effective permeability and the separation performance for both species. Since the mass diffusivity and solubility coefficient of both components in the polymeric membrane are required, the experimental data of a commercial Polydimethylsiloxane (PDMS)

membrane were considered. The simulation parameters and details for this analysis are summarized in Table 3.3. In this investigation, it was assumed that, given the concentrations within the membrane are relatively low, there are no interactions effects between the two migrating species [1]. Since the Knudsen diffusion mechanism is assumed to prevail within the nanotubes, water molecules having a smaller molecular weight should diffuse faster through the filler. Therefore, by rotating the nanotubes from a horizontal to a vertical orientation, the effective permeability of both butanol and water will increase. This increase in effective permeability should enhance the total flux of the membrane. However, if the effective permeability of water increases more than the one of butanol, the separation factor for butanol will unfortunately decrease. Results of this analysis are presented in Figures 3.9 and confirmed what was expected. The relative permeability of water increased by only 3% for vertically-aligned nanotubes whereas it was lower than unity for different orientations. The relative permeability of water decreases to 0.75 for horizontal nanotubes. For butanol, the relative permeability is about 0.88 for vertically-aligned nanotubes and decreases to 0.76 for horizontal nanotubes. Based on the physical data of Table 3.3, it is clear that there would be no advantages to use a MMM with nanotubes for the water-butanol separation. In addition, the butanol selectivity decreases with the addition of nanotubes. For horizontal nanotubes, the selectivity is identical to the one prevailing for the polymeric membrane, but the effective permeability would be lower.

Table 3.3. Summary of simulation details for the continuous and dispersed phases

Temperature (K)	310	
Filler volume fraction (ϕ)	0.1	
Filler aspect ratio (α)	10	
Filler outer diameter (nm)	2.0	
Filler inner diameter(nm)	0.8	
	Water	Butanol
Feed concentration (kg.m$_3$)	992.5	5.0
D_c (m$_2$.s$_{-1}$)	5.27×10^{-10}[1]	7.29×10^{-10} [1]
D_d (m$_2$.s$_{-1}$)	1.6×10^{-7}	7.94×10^{-8}
S_c (g.m$_{-3}$/g.m$_{-3}$)	1.6×10^{-3}[4]	1.46×10^{-2} [4]
S_d (g.m$_{-3}$/g.m$_{-3}$)	4.44×10^{-5}	1.38×10^{-5}
P_c (m$_2$.s$_{-1}$)	8.43×10^{-13}	1.06×10^{-11}
P_d (m$_2$.s$_{-1}$)	7.10×10^{-12}	1.10×10^{-12}
P_d/P_c	8.4	0.1

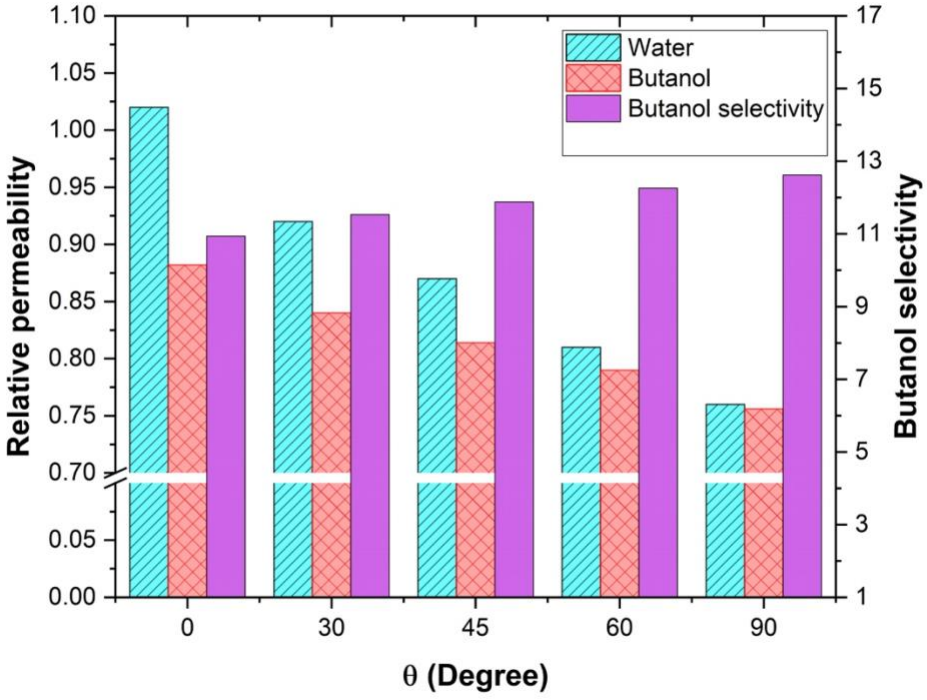

Figure 3.9. Water and butanol relative permeability and butanol selectivity at different orientations of the nanotubes for a length-to-diameter aspect ratio α of 10.

3.3.6 Comparison of the relative permeability with existing models

One of the objectives of this investigation was to assess the accuracy of existing models for the prediction of the relative permeability. Since the correlation proposed by Kang et al. [26] to estimate the effective permeability, referred as the KJN model, is one that considers the orientation of the nanotubes and their diffusion coefficient in the axial direction, it was compared first to the data obtained in this investigation. The KJN model was developed for MMMs with tubular fillers assuming a one-dimensional mass transport. In this section, the relative permeability P_r was calculated using Equations. (3.4)-(3.6) for a MMM with embedded nanotubes with an orientation varying from 0° to 90°, with a constant length-to-diameter aspect ratio of 10 and a filler volume fraction ϕ of 0.1. Results are presented in Figure 3.10 for three values of the permeability ratio

(P_d/P_c). Results show that the KJN model predicts a nearly constant relative permeability over a very large range of orientation and its value only drop at around 80°. In addition, the predicted values of the relative permeability are nearly independent of the permeability ratio. The insensitivity of the KJN model to the permeability ratio is due the predominance of the first term of Equation (3.4) compared to the second term containing the permeability ratio. For a permeability ratio of 1000, the first term varies between 0.9 to 1.0 whereas the second term varies between 0.0001 to 0.001. Comparing the results of the numerical simulations for various values of the relative permeability, it is obvious that the KJN model cannot predict adequately the relative permeability of mixed matrix membranes with nanotube fillers.

Since unreliable predictions were obtained with the KJN model, it was decided to perform a similar comparison with other models that had the most predictive potential. The Maxwell model and the Hamilton-Crosser model were retained for this additional comparison. The Maxwell model was derived for MMMs containing spherical fillers with isotropic diffusivity, whereas the Hamilton-Crosser model was developed for MMMs with tubular fillers. The relative permeability P_r calculated by the two models and compared to the numerical results for vertically-aligned tubular fillers with a constant length-to-diameter aspect ratio of 100 and three values of the permeability ratio (P_d/P_c) (10, 100 and 1000). Results of this study are presented in Figure 3.11. For a permeability ratio of 10 (Figure 3.11(a)), the diffusion barrier effect of the impermeable side wall of the nanotubes perpendicular to the main direction of the migrating species is more significant than the enhancement of the higher permeability in the axial direction. This diffusion barrier of the nanotube wall is only considered by the numerical method. As a result, the three models over predict the relative permeability for this lower permeability ratio. Results for higher (P_d/P_c) ratios of 100 (Figure 3.11(b)) and 1000 (Figure 3.11(c)), Maxwell and KJN models underestimate the results while the Hamilton-Crosser model over predicts the relative permeability. Even though the Maxwell model underestimates the relative permeability, at a lower nanotube volume fraction and an intermediate permeability ratio (P_d/P_c = 100), it provides a relatively better prediction. Therefore, additional numerical simulations were performed to calculate the relative permeability as a function of the filler volume fraction with a permeability ratio of 100 for three length-to-diameter aspect ratio (α of 10, 20 and 50). The numerical results are compared on Figure 3.12 with the three prediction models. At lower aspect ratio (α = 10), both the Maxwell and Hamilton-Crosser models predict a higher relative permeability than the numerical simulations.

On the other hand, for α of 20 and 50, results of Figures 3.12(b) and 3.12(c) show that the numerically predicted relative permeability fell between the Hamilton-Crosser and Maxwell model predictions. However, the difference in P_r between the present work and the estimations by the Maxwell model is relatively small for P_d/P_c = 100 and α = 10 and 20, but it becomes more pronounced for higher values of P_d/P_c and α. According to the all comparisons in this section, there is obviously a need to develop a new correlation that will provide more accurate predictions of the relative permeability of MMMs embedding nanotube fillers.

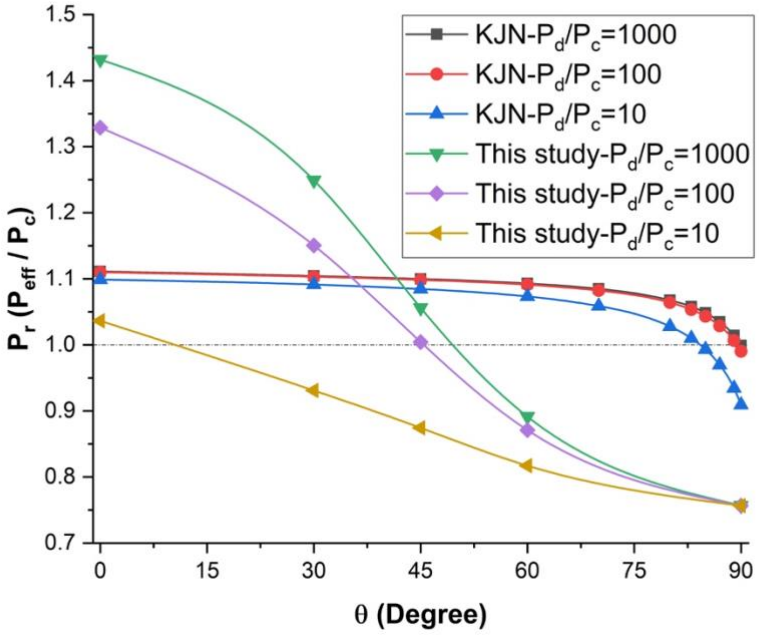

Figure 3.10. Comparison of the relative permeability predicted by the numerical simulations with the KJN model as a function of the nanotube orientation for three permeability ratios at ϕ = 0.1 and α = 10.

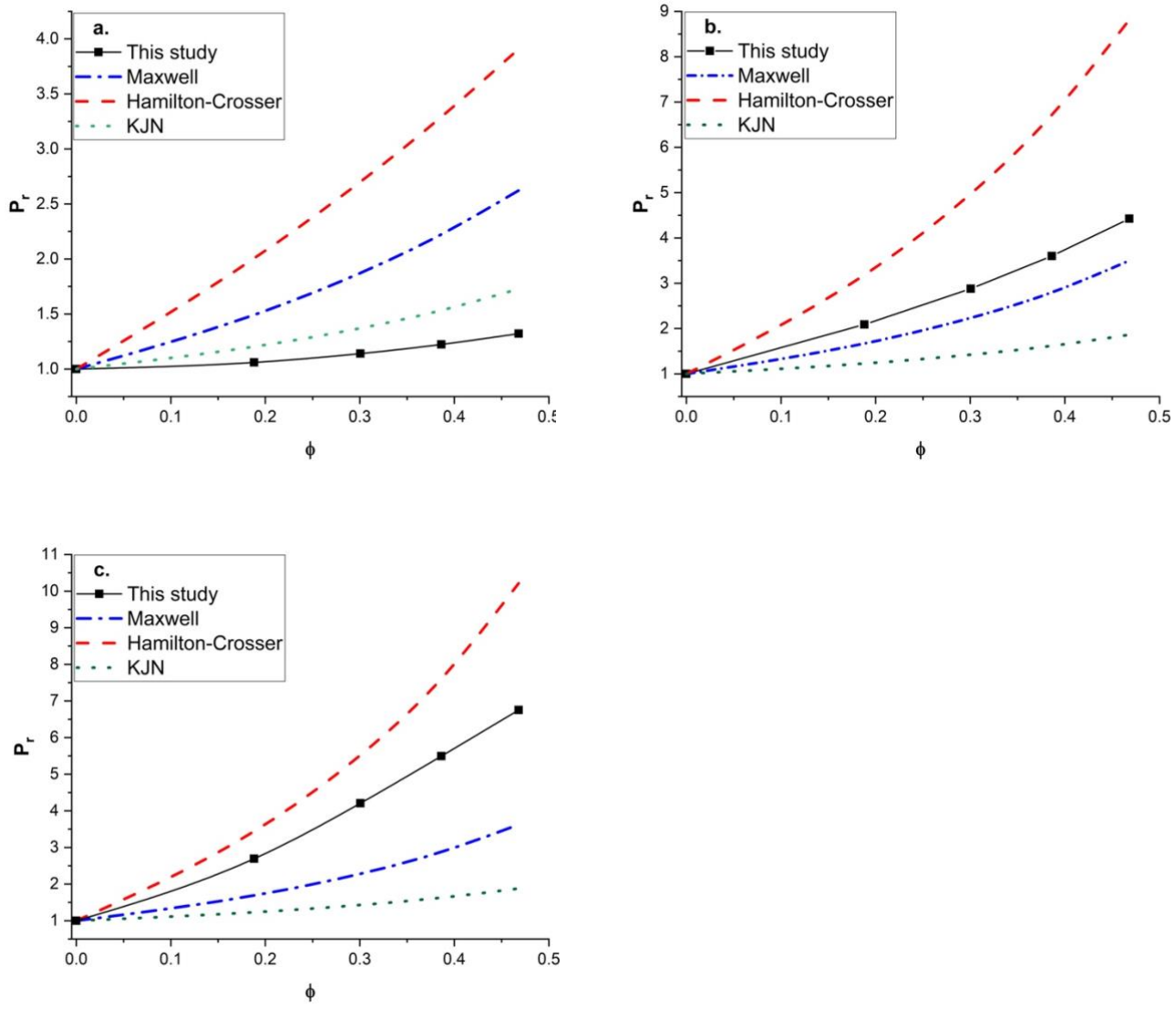

Figure 3.11. Comparison of the predicted relative permeability obtained in this study with the Maxwell, Hamilton-Crosser and KJN models as a function of the nanotube volume fraction for α = 100: **a)** (P_d/P_c) = 10, **b)** (P_d/P_c) = 100, **c)** (P_d/P_c) = 1000.

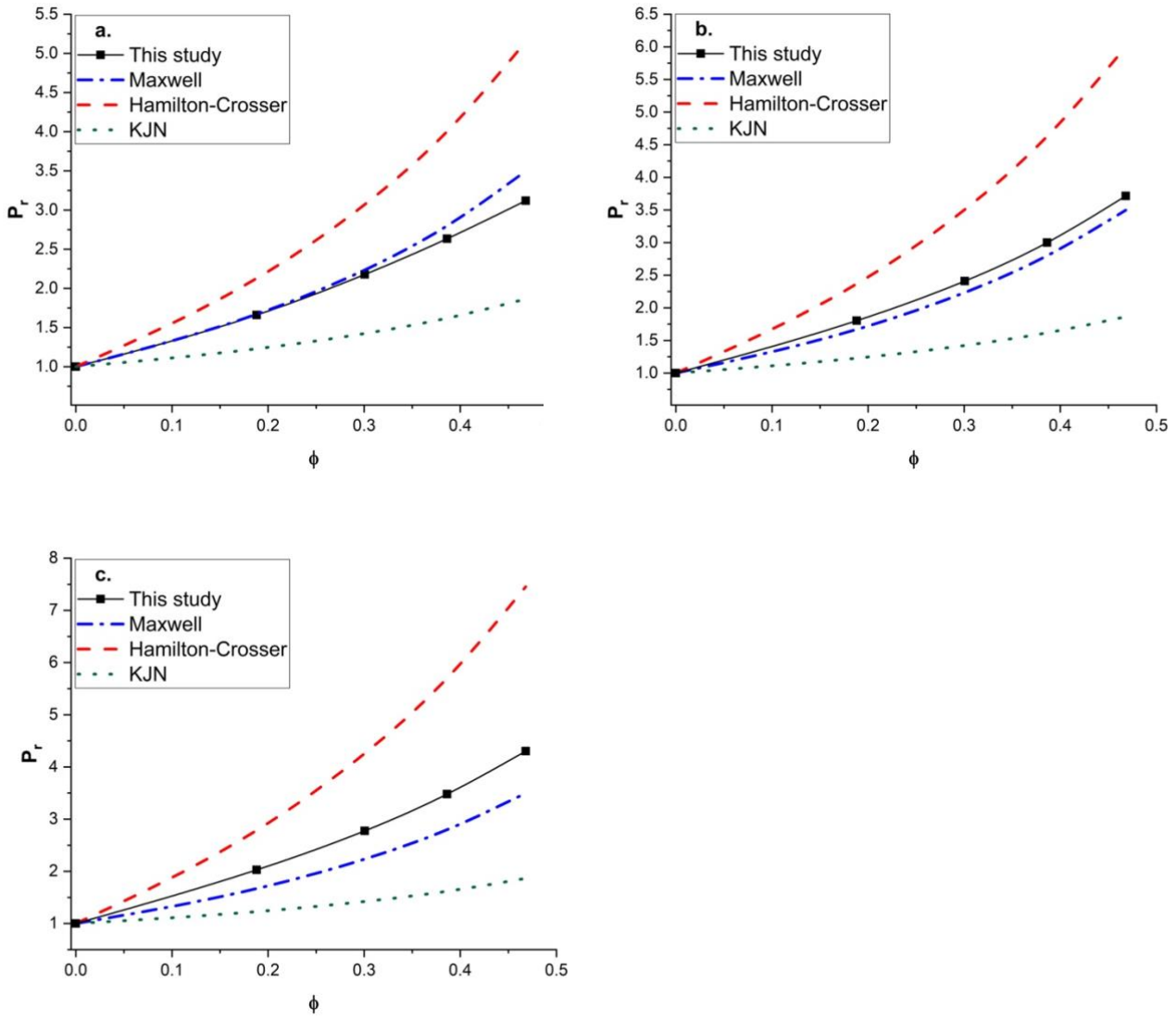

Figure 3.12. Comparison of the predicted relative permeability obtained in this study with the Maxwell, Hamilton-Crosser and KJN models as a function of the nanotube volume fraction for (P_d/P_c) = 100: **a)** α = 10, **b)** α = 20, **c)** α = 50.

3.4 Conclusion

The Fickian diffusion equation was solved numerically for estimating the effective permeability of MMMs with tubular fillers. The numerical model explicitly accounts for the effects of the filler permeability, volume fraction, aspect ratio, and orientation. Several general conclusions can be drawn from this study. First, the filler orientation has an enormous effect on the mixed matrix membrane effective permeability and aligning the fillers vertically is very favourable. Second, in the vertical-aligned applications, fillers with higher aspect ratios are more beneficial to MMMs and significantly increase the effective permeability. Third, fillers with low dispersed-to-continuous phase permeability ratio, ($P_d/P_c<10$) should be avoided in fabrication of mixed matrix membranes due to the significant diffusion barrier effect of the impermeable side wall of the nanotubes perpendicular to the main direction of the migrating species which is more than the enhancement of the higher permeability in the axial direction. On the other hand, fillers with lower outside-to-inside diameter ratio are more advantageous. Finally, existing analytical models for the prediction of the relative permeability of MMMs with tubular fillers are not reliable. Therefore, there is a need to develop a new correlation that would provide more accurate predictions of the relative permeability of MMMs embedding nanotube fillers.

Acknowledgements

Financial support received from NSERC (Natural Sciences and Engineering Research Council) of Canada is gratefully acknowledged.

Abbreviations

CNT	Carbon nanotube
FD	Finite difference
KJN	Kang-Jones-Nair
MMM	Mixed matrix membrane
MOF	Metal-organic framework
PDC	Periodic boundary condition

PDMS	Polydimethylsiloxane

Nomenclatures

C	Concentration ($kg.m^{-3}$)
D	Diffusion coefficient ($m^2.s^{-1}$)
d_i	Inner diameter of filler nanotube (nm)
d_o	Outer diameter of filler nanotube (nm)
J	Permeate flux ($kg.m^{-2}.s^{-1}$)
L	Length of nanotube filler (nm)
L_1	Size of the unit element in x-direction (nm)
L_2	Size of the unit element in y-direction (nm)
L_3	Size of the unit element in z-direction (nm)
M	Molecular weight ($kg.kmol^{-1}$)
N	Number of nodes in simulation domain
n	Shape factor
P	Permeability ($m^2.s^{-1}$)
R	Gas constant ($J.K^{-1}.mol^{-1}$)
S	Solubility factor ($g.m^{-3}/g.m^{-3}$)
t	Time (s)
T	Temperature (K)
x	x coordinate

y	y coordinate
z	z coordinate
α	Nanotube filler aspect ratio
θ	Angle of filler orientation
ψ	Sphericity
$\emptyset$	Volumetric Filler Content

Superscripts

L	Left
R	Right

Subscripts

c	Continuous phase
d	Dispersed phase
eff	Effective
f	Feed
K	Knudsen diffusion
m	Component
r	Relative
t	total

References

[1] A. Ebneyamini, H. Azimi, F.H. Tezel, J. Thibault, Modelling of mixed matrix membranes: Validation of the resistance-based model, J. Memb. Sci. 543 (2017) 361–369. doi:10.1016/j.memsci.2017.08.064.

[2] H. Vinh-Thang, S. Kaliaguine, Predictive Models for Mixed-Matrix Membrane Performance: A Review, Chem. Rev. 113 (2013) 4980–5028. doi:10.1021/cr3003888.

[3] H. Azimi, A. Ebneyamini, F.H. Tezel, J. Thibault, Separation of organic compounds from ABE model solutions via pervaporation using activated carbon/PDMS mixed matrix membranes, Membranes (Basel). 8 (2018) 1–15. doi:10.3390/membranes8030040.

[4] H. Azimi, F.H. Tezel, J. Thibault, Effect of embedded activated carbon nanoparticles on the performance of polydimethylsiloxane (PDMS) membrane for pervaporation separation of butanol, J. Chem. Technol. Biotechnol. 92 (2017) 2901–2911. doi:10.1002/jctb.5306.

[5] D. Carter, F.H. Tezel, B. Kruczek, H. Kalipcilar, Investigation and comparison of mixed matrix membranes composed of polyimide matrimid with ZIF – 8, silicalite, and SAPO – 34, J. Memb. Sci. 544 (2017) 35–46. doi:10.1016/j.memsci.2017.08.068.

[6] R.W. Baker, Future directions of membrane gas separation technology, Ind. Eng. Chem. Res. 41 (2002) 1393–1411. doi:10.1021/ie0108088.

[7] A. Babin, F. Bougie, D. Rodrigue, M.C. Iliuta, A closer look on the development and commercialization of membrane contactors for mass transfer and separation processes, Sep. Purif. Technol. 227 (2019). doi:10.1016/j.seppur.2019.115679.

[8] A. Ebneyamini, H. Azimi, F.H. Tezel, J. Thibault, Mixed matrix membranes applications: Development of a resistance-based model, J. Memb. Sci. 543 (2017) 351–360. doi:10.1016/J.MEMSCI.2017.08.065.

[9] G. Liu, W.S. Hung, J. Shen, Q. Li, Y.H. Huang, W. Jin, K.R. Lee, J.Y. Lai, Mixed matrix membranes with molecular-interaction-driven tunable free volumes for efficient bio-fuel recovery, J. Mater. Chem. A. 3 (2015) 4510–4521. doi:10.1039/c4ta05881j.

[10] D. Yang, C. Cheng, M. Bao, L. Chen, Y. Bao, C. Xue, The pervaporative membrane with vertically aligned carbon nanotube nanochannel for enhancing butanol recovery, J. Memb. Sci. 577 (2019) 51–59. doi:10.1016/j.memsci.2019.01.032.

[11] P. Shao, A. Kumar, Separation of 1-butanol/2,3-butanediol using ZSM-5 zeolite-filled polydimethylsiloxane membranes, J. Memb. Sci. 339 (2009) 143–150. doi:10.1016/J.MEMSCI.2009.04.042.

[12] W.S. Chi, B.J. Sundell, K. Zhang, D.J. Harrigan, S.C. Hayden, Z.P. Smith, Mixed-Matrix Membranes Formed from Multi-Dimensional Metal–Organic Frameworks for Enhanced Gas Transport and Plasticization Resistance, ChemSusChem. 12 (2019) 2355–2360. doi:10.1002/cssc.201900623.

[13] A. Nouri, R. Yavari, M. Aroon, T. Yousefi, Multiwalled Carbon Nanotubes / Polyethersulfone Mixed Matrix Nanofiltration Membrane for the removal of cobalt ion, 4 (2019) 97–108. doi:10.22090/jwent.2019.02.002.

[14] R. Borgohain, N. Jain, B. Prasad, B. Mandal, B. Su, Carboxymethyl chitosan/carbon nanotubes mixed matrix membranes for CO2 separation, React. Funct. Polym. (2019) 104331. doi:10.1016/j.reactfunctpolym.2019.104331.

[15] Q. Xin, Y. Gao, X. Wu, C. Li, T. Liu, Y. Shi, Y. Li, Z. Jiang, H. Wu, X. Cao, Incorporating one-dimensional aminated titania nanotubes into sulfonated poly(ether ether ketone) membrane to construct CO_2-facilitated transport pathways for enhanced CO_2 separation, J. Memb. Sci. 488 (2015) 13–29. doi:10.1016/j.memsci.2015.02.047.

[16] S.A. Hashemifard, A.F. Ismail, T. Matsuura, Mixed matrix membrane incorporated with large pore size halloysite nanotubes (HNTs) as filler for gas separation: Morphological diagram, Chem. Eng. J. 172 (2011) 581–590. doi:10.1016/j.cej.2011.06.031.

[17] R. Surya Murali, M. Padaki, T. Matsuura, M.S. Abdullah, A.F. Ismail, Polyaniline in situ modified halloysite nanotubes incorporated asymmetric mixed matrix membrane for gas separation, Sep. Purif. Technol. 132 (2014) 187–194. doi:10.1016/j.seppur.2014.05.020.

[18] L. Yang, S. Zhang, H. Wu, C. Ye, X. Liang, S. Wang, X. Wu, Y. Wu, Y. Ren, Y. Liu, N. Nasir, Z. Jiang, Porous organosilicon nanotubes in pebax-based mixed-matrix membranes for biogas purification, J. Memb. Sci. (2019) 301–308. doi:10.1016/j.memsci.2018.12.018.

[19] J. Zang, S. Konduri, S. Nair, D.S. Sholl, Self-diffusion of water and simple alcohols in single-walled aluminosilicate nanotubes, ACS Nano. 3 (2009) 1548–1556. doi:10.1021/nn9001837.

[20] S. Konduiri, H.M. Tong, S. Chempath, S. Nair, Water in single-walled aluminosilicate nanotubes: Diffusion and adsorption properties, J. Phys. Chem. C. 112 (2008) 15367–15374. doi:10.1021/jp8025144.

[21] L. Dumee, L. Velleman, K. Sears, M. Hill, J. Schutz, N. Finn, M. Duke, S. Gray, Control of porosity and pore size of metal reinforced carbon nanotube membranes, Membranes (Basel). 1 (2010) 25–36. doi:10.3390/membranes1010025.

[22] J.Y. Kim, K.H. Kim, K.B. Kim, Fabrication and electrochemical properties of carbon nanotube/polypyrrole composite film electrodes with controlled pore size, J. Power Sources. 176 (2008) 396–402. doi:10.1016/j.jpowsour.2007.09.117.

[23] D.Y. Kang, J. Zang, C.W. Jones, S. Nair, Single-walled aluminosilicate nanotubes with organic-modified interiors, J. Phys. Chem. C. 115 (2011) 7676–7685. doi:10.1021/jp2010919.

[24] J. Zang, S. Chempath, S. Konduri, S. Nair, D.S. Sholl, Flexibility of ordered surface hydroxyls influences the adsorption of molecules in single-walled aluminosilicate nanotubes, J. Phys. Chem. Lett. 1 (2010) 1235–1240. doi:10.1021/jz100219q.

[25] A.F. Ismail, P.S. Goh, S.M. Sanip, M. Aziz, Transport and separation properties of carbon nanotube-mixed matrix membrane, Sep. Purif. Technol. 70 (2009) 12–26. doi:10.1016/j.seppur.2009.09.002.

[26] D.Y. Kang, C.W. Jones, S. Nair, Modeling molecular transport in composite membranes with tubular fillers, J. Memb. Sci. 381 (2011) 50–63. doi:10.1016/j.memsci.2011.07.015.

[27] E. Chehrazi, M. Raef, M. Noroozi, M. Panahi-Sarmad, A theoretical model for the gas permeation prediction of nanotube-mixed matrix membranes: Unveiling the effect of interfacial layer, J. Memb. Sci. 570–571 (2019) 168–175. doi:10.1016/j.memsci.2018.10.038.

[28] T.P. Wang, D.Y. Kang, Predictions of effective diffusivity of mixed matrix membranes with tubular fillers, J. Memb. Sci. 485 (2015) 123–131. doi:10.1016/j.memsci.2015.03.028.

[29] A.I. Skoulidas, D.M. Ackerman, J.K. Johnson, D.S. Sholl, Rapid Transport of Gases in Carbon Nanotubes, Phys. Rev. Lett. 89 (2002) 13–16. doi:10.1103/PhysRevLett.89.185901.

[30] J.D. Felske, Effective thermal conductivity of composite spheres in a continuous medium with contact resistance, Int. J. Heat Mass Transf. 47 (2004) 3453–3461. doi:10.1016/j.ijheatmasstransfer.2004.01.013.

[31] S.A. Hashemifard, A.F. Ismail, T. Matsuura, Prediction of gas permeability in mixed matrix membranes using theoretical models, J. Memb. Sci. 347 (2010) 53–61. doi:10.1016/j.memsci.2009.10.005.

[32] D.Q. Vu, W.J. Koros, S.J. Miller, Mixed matrix membranes using carbon molecular sieves: II. Modeling permeation behavior, J. Memb. Sci. 211 (2003) 335–348. doi:10.1016/S0376-7388(02)00425-8.

[33] M.A. Aroon, A.F. Ismail, T. Matsuura, M.M. Montazer-Rahmati, Performance studies of mixed matrix membranes for gas separation: A review, Sep. Purif. Technol. 75 (2010) 229–242. doi:10.1016/j.seppur.2010.08.023.

[34] R.H.B. Bouma, A. Checchetti, G. Chidichimo, E. Drioli, Permeation through a heterogeneous membrane: The effect of the dispersed phase, J. Memb. Sci. 128 (1997) 141–149. doi:10.1016/S0376-7388(96)00303-1.

[35] R.L. Hamilton, Thermal conductivity of heterogeneous two-component systems, Ind. Eng. Chem. Fundam. 1 (1962) 187–191. doi:10.1021/i160003a005.

Chapter 4:

Conclusions and recommendations

In the first part of this study, effect of the particle size and mass fraction of ZIF-8 on the performance PDMS/ZIF-8 MMM for the separation of butanol from aqueous binary solutions was investigated. Among the three different sizes of ZIF-8 nanoparticles (30, 65, and 80 nm), the small-size ZIF-8 showed the best results at 8 wt% loading content in MMM with an increase of 350% and 6% in total permeation flux and butanol selectivity, respectively, compared to the neat PDMS membrane. The results revealed the importance of particle size and interface compatibility between the filler and the polymer chains in the performance of mixed matrix membranes. Fillers with smaller particle size can provide more surface area and better polymer compatibility. On the other hand, bigger fillers or fillers with complex geometry are responsible for creating defects and reduce the MMMs performance.

In the second part of this study, a series of numerical simulations were performed to solve the Fick's second law of diffusion to determine the concentration profiles in MMMs with tubular fillers in order to gain a deeper understanding on the effect of numerous physical parameters on the estimation of the effective permeability of the MMMs. The results show that the filler orientation has an enormous effect on the mixed matrix membrane effective permeability and aligning the tubular fillers in the direction of the main species permeation was very favourable. This effect was amplified by increasing the nanotube volume fraction. In addition, for vertical-aligned nanotubes, fillers with a higher length-to-diameter aspect ratio had higher effective permeability. Finally, fillers with low dispersed-to-continuous phase permeability ratio, ($P_d/P_c<10$) should be avoided in fabrication of mixed matrix membranes. On the other hand, fillers with lower outside-to-inside diameter ratio would be more advantageous.

According to the results obtained in this study, future works should be directed towards more compatible smaller particles. Particles such as carbon quantum dots (C dots) and graphene oxides (GOs) could be perfect candidates for this application and should be tested. In addition, fillers with spherical shape and good compatibility with PDMS such as lignin have the potential to improve MMMs performance and are highly recommended.

Furthermore, nanotubes need a more comprehensive investigation for both numerical and experimental methods. Existing analytical models for the prediction of the relative permeability of MMMs with tubular fillers are not reliable. Therefore, the approach and data provided by this study can be used to develop a new correlation that would provide more accurate predictions of the relative permeability of MMMs embedding nanotube fillers.